J. Fluid Mech. (1995), *vol.* 290, *pp.* 131–166

Strongly nonlinear interfacial dynamics in core–annular flows

By V. KERCHMAN†
10201 Bustleton C-53, Philadelphia, PA 19116, USA

(Received 18 March 1994 and in revised form 25 November 1994)

Nonlinear stability of a pressure driven core–annular flow is analysed, and a study of the large-amplitude interfacial dynamics is reported in the limit of a small ratio β of the annular clearance to the radius. An asymptotic nonlinear evolution equation for the annular film thickness is derived as a general case which involves shear coupling with the core flow. We discuss the effects of the surface tension parameter and viscosity stratification of various orders in β. The governing equation is investigated by solving it on extended intervals. Long-term simulations in a wide range of parameters reveal rich dynamics of wave patterns and coherent structures. Only in a narrow window of the small control parameters can it be described by the weakly nonlinear dissipative–dispersive equation, exhibiting behaviour of strictly bounded solutions which varies from a spatiotemporal chaos to the quasi-steady wavetrains. For sufficiently high surface tension, some pulses (to which the primary instabilities saturate) can coalesce into stable larger structures. This leads to the formation of solitary humps via cascade absorption. Substantial thickness non-uniformities can cause collapse of the perfect CAFF owing to the lens formation or extreme film thinning. Our critical value of the control parameter is in good agreement with the experimental data by Aul & Olbricht. Under strong coupling of the core flow with a less viscous annular film the interfacial evolution settles to a train of inverted pulses. Long-time behaviour in the intermediate range of parameters is diversified from regular pulse trains, to the formation of wide multi-peak structures or blow-up, depending on the apparent involvement of the core.

1. Introduction

Analysis of a slow viscous flow of two immiscible fluids within a tube is important for understanding the mobility of oil–aqueous solution mixtures in porous media (in particular, in the process of oil recovery by its displacement). Typically, a thin film of oil is wetting the inner surface of the tube, and the central part is occupied by a less viscous fluid. Aul & Olbricht (1990) conducted experiments on low-Reynolds-number, pressure-driven flow in a glass capillary tube with thin annular oil film, and observed development and motion of axisymmetric lobes of the thin film fluid. Similar configurations appear in modeiling the dynamics of a thin liquid film that covers the inner surface of the lung airways studied by Johnson *et al.* (1991) and Halpern & Grotberg (1992) in the absence of imposed flow. In both problems slow flow is strongly affected by capillary instability of the film–inner fluid interface known since works by Plateau and Rayleigh (see Rayleigh 1902; Goren 1962). Its development may cause closing of the tube via 'pinch-off' of the core fluid and rearrangement of the thickened

† Present address: Goodyear Tire & Rubber Company, GTC 431A, Akron, OH 44309-3531, USA.

film portions into lenses, as observed in experiments by Gauglitz & Radke (1988) and Aul & Olbricht (1990), the critical thickness is about 0.1 of the tube radius.

The general formulation of the problem falls within the framework of a core–annular flow (CAF) theory which has attracted a great deal of attention during the past decade. This theory was motivated by an interest in the lubricated pipelining of very viscous crude oil (Ooms *et al.* 1984; Joseph & Renardy 1993; Miesen *et al.* 1992). Hickox (1971) studied effects of viscosity and density stratification on the stability of CAF to long-wave disturbances. Joseph and collaborators carried out a comprehensive numerical and asymptotic analysis of linear stability of CAFs, summarized in a book by Joseph & Renardy (1993), where results of experiments by Bai, Chen & Joseph (1992) are presented as well. In the case of a narrow annular region occupied by a less viscous fluid, Preziosi, Chen & Joseph (1989) found that strong viscosity stratification can suppress capillary instability but only for sufficiently large Reynolds number. Georgiou *et al.* (1992) conducted an asymptotic investigation of stability in the limit of thin annulus (CA film flow) for the case when the viscosity ratio is large compared to the film thickness ratio.

Frenkel *et al.* (1987) carried out a weakly nonlinear analysis (for slow flow of the core and the film of the same viscosity) when the imposed flow is strong enough to keep interfacial disturbances much smaller than the unperturbed film thickness which lead to the Kuramoto–Sivashinsky evolution equation. Frenkel (1988) extended this long-wave approach to incorporate viscosity stratification and inertia of the core flow, and obtained a small-amplitude equation with an additional linear term which contributes to dispersive and dissipative effects. Papageorgiou, Maldarelli & Rumschitzki (1990) gave a more systematic exposition and numerical solutions. Their simulations demonstrate the 'regularizing' effect of dispersion (a simpler treatment which directly relates this case to the dissipative–dispersive equation by Kawahara (1983) is given in §6 below).

Hammond (1983) derived an asymptotic nonlinear equation describing large-amplitude development of the thin annular film distortions in the absence of imposed flow. Gauglitz & Radke (1988) extended his analysis using a more accurate (but asymptotically inconsistent) approximation for the surface-tension boundary conditions to simulate bridge formation in thicker films. An equation describing the strongly undulating interface of a film flowing down a cylinder was obtained by Frenkel (1992) (and it may be considered as a thin annulus limit of the long-wave equation by Lin & Liu 1975). In its analysis by Kerchman & Frenkel (1994) different regimes of evolution were discovered, and they are in good quantitative agreement with phenomena observed in experiments by Quéré (1990).

The leading-order nonlinear interfacial equation for low Reynolds numbers CA film flow with strong surface tension is derived in §3 in a general case with significant shear coupling between annular and core fluids. In §4 we present extensive numerical study of the case when this coupling can be neglected (see also Frenkel & Kerchman 1994). It demonstrates dynamics of pulse-like coherent structures engaged in various interactions, which in certain aspects is parallel to that in Kerchman & Frenkel (1994). Isolated pulses can be described in terms of spatially periodic travelling waves which are briefly considered in §5. The weakly nonlinear case and strongly nonlinear regimes when the interfacial shear plays essential role are studied in §6. In §7 we summarize and discuss results and their interpretation.

2. Formulation of the problem

We consider pressure-driven core–annular flow of two immiscible fluids through a straight circular tube. All dimensional variables below are marked by overbars. In undisturbed flow the core region $0 \leqslant \bar{r} \leqslant \bar{R}_i$ is occupied by a fluid with viscosity $\bar{\mu}_1$, and thin annular film of the second fluid with viscosity $\bar{\mu}_2$ is located in $\bar{R}_1 \leqslant \bar{r} \leqslant \bar{R}_2$. Constant pressure gradient $\bar{F} = -\mathrm{d}\bar{P}_1/\mathrm{d}\bar{z} = -\mathrm{d}\bar{P}_2/\mathrm{d}\bar{z}$ drives the flow. We use dimensionless variables by scaling lengths with the radius $\bar{R}_1$: $r = \bar{r}/\bar{R}_1$, $z = \bar{z}/\bar{R}_1$, velocities with the centreline velocity

$$\bar{W}_c = \bar{F}\{\bar{R}_1^2(\bar{\mu}_2 - \bar{\mu}_1) + \bar{R}_2^2\bar{\mu}_1\}/4\bar{\mu}_1\bar{\mu}_2,$$

and time with $\bar{R}_1/\bar{W}_c$. Pressures are measured with $\bar{\rho}_1\,\bar{W}_c^2$ (and for simplicity we consider mostly the case of equal densities $\bar{\rho}_1 = \bar{\rho}_2$).

The undisturbed thickness ratio is defined as $\beta = (\bar{R}_2 - \bar{R}_1)/\bar{R}_1$ (2β is the specific film volume for $\beta \ll 1$), and other dimensionless parameters of the problem are the viscosity ratio $m = \bar{\mu}_2/\bar{\mu}_1$, formal Reynolds numbers $\mathbb{R}_l = \bar{\rho}_l\,\bar{W}_c\,\bar{R}_l/\bar{\mu}_l$ ($l = 1, 2$; and thus $\mathbb{R}_1 = m\mathbb{R}_2$), and the dimensionless surface tension

$$\sigma = \frac{\bar{\sigma}}{\bar{\rho}_1\,\bar{R}_1\,\bar{W}_c^2}\left(= \frac{\mathbb{J}}{\mathbb{R}_1^2}\right), \tag{2.1}$$

where $\mathbb{J} = \bar{\rho}_1\,\bar{\sigma}\bar{R}_1/\bar{\mu}_1^2$ is a related parameter independent of $\bar{W}_c$ (Joseph & Renardy 1993).

We can conveniently rewrite the dimensionless equations in a reference frame connected with the undisturbed interface, in which the basic steady flow is given by

$$W(r) = \begin{cases} W_1 = m(1-r^2)/(a^2+m-1) & (0 \leqslant r \leqslant 1), \\ W_2 = (1-r^2)/(a^2+m-1) & (1 \leqslant r \leqslant a = 1+\beta). \end{cases} \tag{2.2}$$

The interface velocity with respect to the wall is $W_{if} = (a^2-1)/(a^2+m-1)$ ($\approx 2\beta/(2\beta+m)$ for $\beta \ll 1$), and effective Reynolds number of the undisturbed film flow is $\mathbb{R}_f = \mathbb{R}_2\,\beta W_{if}$.

We consider only dominant axisymmetric disturbances. The total velocities are written as $\{u_l,\ W_l + w_l\}$, and the total pressures as $P_l + p_l$ ($l = 1, 2$). The exact nonlinear equations for the perturbations are

$$r^{-1}\,\partial_r(ru_l) + \partial_z\,w_l = 0, \tag{2.3a}$$

$$\partial_t\,u_l + u_l\,\partial_r\,u_l + W_l(r)\,\partial_z\,u_l + w_l\,\partial_z\,u_l = -\partial_r\,p_l + \mathbb{R}_l^{-1}\nabla^2 u_l, \tag{2.3b}$$

$$\partial_t\,w_l + u_l(W_l' + \partial_r\,w_l) + (W_l + w_l)\,\partial_z\,w_l = -\partial_z\,p_l + \mathbb{R}_l^{-1}\nabla^2 w_l. \tag{2.3c}$$

Here $W_l' = \mathrm{d}W_l/\mathrm{d}r$. Boundary conditions are no-slip at the wall

$$u_2 = w_2 = 0, \quad r = 1+\beta. \tag{2.4}$$

The perturbed interface is described by a deflection function $\eta(z, t)$

$$r_{if} = 1 - \beta\eta, \tag{2.5}$$

and thus the scaled annular film thickness

$$h = (\bar{R}_2 - \bar{R}_{if})/(\bar{R}_2 - \bar{R}_1) = 1 + \eta. \tag{2.6}$$

We are focused on the analysis of nonlinear stability when the annular film is thin: $\beta \ll 1$, but not limited to the case of small interfacial perturbations $\eta = O(\beta)$ considered

by Frenkel *et al.* (1987), Frenkel (1988), and Papageorgiou, Maldarelli & Rumschitzki (1990). The decomposition of the total velocities into basic velocities (2.3) and their perturbations is generally by convention, because they can be of the same order. It makes the derivation easier (and the comparative analysis in a special case of small amplitudes as well).

The conditions at the interface are as follows (where derivatives of η are denoted by subscripts z and t):

the continuity of velocities:

$$u_1 = u_2, \quad W_1 + w_1 = W_2 + w_2, \tag{2.7}$$

the continuity of tangential stress:

$$m\{(W_2' + \partial_r w_2 + \partial_z u_2)[1 - \beta^2(\eta_z)^2] - 2\beta\eta_z(\partial_r u_2 - \partial_z w_2)\}$$
$$= (W_1' + \partial_r w_1 + \partial_z u_1)[1 - \beta^2(\eta_z)^2] - 2\beta\eta_z(\partial_r u_1 - \partial_z w_1),$$

which may be simplified for small β to

$$\partial_z u_1 + \partial_r w_1 - 2\beta\eta_z(\partial_r u_1 - \partial_z w_1) = m(\partial_z u_2 + \partial_r w_2), \tag{2.8}$$

because $[mW_2' - W_1']$ vanishes identically; the condition for the jump of the normal stress:

$$[P_1 + p_1 - 2\mathbb{R}_1^{-1}\partial_r u_1 - P_2 - p_2 + 2\mathbb{R}_2^{-1}\partial_r u_2][1 + \beta^2(\eta_z)^2]$$
$$-[2\mathbb{R}_1^{-1}(\partial_z u_1 + W_1' + \partial_r w_1) - 2\mathbb{R}_2^{-1}(\partial_z u_2 + W_2' + \partial_r w_2)]\beta\eta_z$$
$$= \sigma\left[\beta\eta_{zz} + \frac{1 + \beta^2(\eta_z)^2}{1 - \beta\eta}\right][1 + \beta(\eta_z)^2]^{-3/2}, \tag{2.9}$$

and finally, the kinematic condition at the interface:

$$\beta[\eta_t + (W + w)\eta_z] = -u \tag{2.10}$$

3. Leading-order equation for the interface

We consider asymptotic expansions of solutions for small thickness ratio β in the conditions of low-Reynolds-number flow. The surface-tension parameter σ is assumed to be large enough with respect to β^{-1}, and therefore according to the linear stability analysis by Joseph and his co-workers (Joseph & Renardy 1993) confirmed in Georgiou *et al.* (1992), criteria for the initial development of interfacial disturbances are essentially the same as in classic Rayleigh theory for viscous threads and annular films without imposed flow (see e.g. Goren 1962; Hammond 1983). Disturbances with wavelengths larger than the circumference of the unperturbed interface are unstable and the fastest growing modes are about $\sqrt{2}$ of this critical length – thus a primary characteristic scale along the tube is of the order of core radius (one in our dimensionless units).

Simplified equations for thin annular film are similar to those of lubrication theory, with the perturbation flow driven primarily by 'large' pressure perturbations at the distorted interface as (2.9) prescribes. The core flow for $\mathbb{R}_1 \ll 1$ is described by Stokes equations. (The general case $\mathbb{R}_1 \sim 1$ can be considered by means of the Orr–Sommerfeld equation as in Frenkel (1988) and Papageorgiou *et al.* (1990), but only when perturbations of the core flow are small enough to allow linearization.)

Let us introduce the stretched coordinate across the vicinity of the interface (including the entire annular region): $r = 1+\beta y$, so that in the film $-\eta \leqslant y \leqslant 1$. Retention of the few terms in formal expansion of the film flow equations in powers of β yields an extended lubrication approximation

$$\beta^{-1}\partial_y u_2 + \partial_z w_2 = -u_2 + O(\beta u_2), \tag{3.1a}$$

$$\beta^{-2}\partial_{yy}^2 w_2 - \mathbb{R}_2 \partial_z p_2 = -\beta^{-1}\partial_y w_2 + \mathbb{R}_2(W_2 + w_2)\partial_z w_2 + O(w_2), \tag{3.1b}$$

$$\partial_y p_2 = (\beta \mathbb{R}_2)^{-1}\partial_{yy}^2 u_2 + O(u_2). \tag{3.1c}$$

Conditions at the wall are

$$u_2 = w_2 = 0 \quad (y = 1), \tag{3.2}$$

and conditions (2.8)–(2.10) at the interface $y = -\eta$ can be expanded to their leading order in β as

$$u_2 = u_1, \quad w_2 = w_1 + (W_1 - W_2), \tag{3.3}$$

$$\partial_y w_2 = m^{-1}\beta(\partial_r w_1 + \partial_z u_1), \tag{3.4}$$

$$p_2 + \sigma\beta(\eta_{zz} + \eta) + 2\mathbb{R}_2^{-1}\partial_z w_2 = p_1 + 2\mathbb{R}_1^{-1}\partial_z w_1. \tag{3.5}$$

Here for $y = O(1)$

$$W_2(y) = -\frac{2\beta}{2\beta+m}y - \frac{2\beta^2}{2\beta+m}y^2 = -W_{if}y\{1 + O(\beta)\}, \quad W_1(y) = mW_2(y). \tag{3.6}$$

We suppose the surface-tension parameter σ to be large enough that capillary pressures, induced by the interfacial distortions, dominate the perturbation film flow and set orders of magnitudes for velocities u_2, w_2, including the case of sizeable disturbances $\eta = O(1)$, $w_2 = O(W_{if})$. The latter implies a small Goucher number $Go = \bar{R}_1/\bar{\kappa} \sim \mathbb{C}^{1/2}$, where $\bar{\kappa} = (\bar{\sigma}/\bar{F})^{1/2}$ is the capillary length, and $\mathbb{C}$ is the capillary number. From the normal stress condition (3.5), the magnitude of the dimensionless pressure p_2 is of the order $\sigma\beta\eta$. Axial momentum and continuity equations stipulate the respective scales for film velocities: $w_2 = O(\mathbb{R}_2\beta^2 p_2)$ and $u_2 = O(\beta w_2)$. Thus, we can seek asymptotic expansion of the film solution in the form

$$p_2 = \sigma\beta[p^{(0)} + \beta p^{(1)} + \ldots], \tag{3.7a}$$

$$u_2 = \mathbb{R}_2\sigma\beta^4[u^{(0)} + \beta u^{(1)} + \ldots], \tag{3.7b}$$

$$w_2 = \mathbb{R}_2\sigma\beta^3[w^{(0)} + \beta w^{(1)} + \ldots], \tag{3.7c}$$

with the $O(1)$ functions $p^{(0)}$, $u^{(0)}$, $w^{(0)}$.

Leading-order solution to (3.1)–(3.5) satisfies (3.1) with zero right-hand sides, and can be written in a general form which involves coupling with the core flow by means of the perturbation shear strain rate at the interface

$$\gamma = (\partial_r w_1 + \partial_z u_1)_{r=1-\beta\eta}, \tag{3.8}$$

(taken in its leading order), as follows

$$p^{(0)} = -(\eta_{zz} + \eta), \tag{3.9a}$$

$$u^{(0)} = -[\partial_{zz}p^{(0)}]\frac{y^3 - 3y + 2}{6} - \partial_z\left\{\eta p^{(0)} + \frac{\gamma}{\mathbb{R}_1\sigma\beta^2}\right\}\frac{(y-1)^2}{2}, \tag{3.9b}$$

$$w^{(0)} = [\partial_z p^{(0)}]\{\tfrac{1}{2}(y^2 - 1) + \eta(y-1)\} + \frac{\gamma}{\mathbb{R}_1\sigma\beta^2}(y-1). \tag{3.9c}$$

Substitution of (3.9) into (2.10) provides a general form of the evolution equation for disturbed interface

$$\eta_t+\frac{2\beta}{2\beta+m}\eta\eta_z+\tfrac{1}{3}\mathbb{R}_2\sigma\beta^3\{(1+\eta)^3(\eta_z+\eta_{zzz})\}_z-\frac{\beta}{2m}\{\gamma(1+\eta)^2\}_z=0. \tag{3.10}$$

It is convenient to rescale the dimensionless time employing the intrinsic velocity of the unperturbed interface $W_{if}=2\beta/(2\beta+m)$: $t'=W_{if}t$ that brings (3.10) into 'standard' form (and hereinafter primes are dropped)

$$\eta_t+\eta\eta_z+S\{(1+\eta)^3(\eta_z+\eta_{zzz})\}_z-\frac{m+2\beta}{4m}\{\gamma(1+\eta)^2\}_z=0. \tag{3.11}$$

Here
$$S=\tfrac{1}{6}\mathbb{R}_2\sigma\beta^2(2\beta+m)=\tfrac{1}{3}\mathbb{R}_f\sigma_f\beta^2 \tag{3.12}$$

(where $\sigma_f=\bar{\sigma}/(\bar{\rho}_2\bar{R}_1\bar{W}_{if}^2)$).

The control parameter S is of the order one or higher (it can be of the order β^q for some positive $q<2$). Applicability of (3.9)–(3.11) is limited by a condition that the core perturbations do not play a predominating role: $\gamma\sim\mathbb{R}_1\sigma\beta^2\eta$ at most.

Derivation can be completed by expressing (or estimating) the last summand in (3.11) in terms of the interfacial deviation η over the specific parameter ranges.

The core solution may be treated using a perturbation stream function Ψ_1

$$u_1=-\partial_z\Psi_1,\quad w_1=r^{-1}\Psi_1+\partial_r\Psi_1, \tag{3.13}$$

and thus the interfacial shear (3.8) can be written as

$$\gamma=[(\partial_{rr}^2+r^{-1}\partial_r-r^{-2}-\partial_{zz}^2)\Psi_1]_{r=1-\beta\eta}. \tag{3.14}$$

We can expand Ψ_1 in powers of β

$$\Psi_1=\psi^{(0)}+\beta\psi^{(1)}+\dots. \tag{3.15}$$

Functions $\psi^{(0)},\psi^{(1)},\dots,$ satisfy the Stokes equation

$$\mathrm{D}^2\psi^{(n)}=0\quad(\mathrm{D}=\partial_{rr}+r^{-1}\partial_r-r^{-2}+\partial_{zz}), \tag{3.16}$$

and the conditions of sewing together with the film solution at the interface (3.3), that is at $r=r_{if}$

$$\partial_z\Psi_1=-3S\beta W_{if}[u^{(0)}|_{y=-\eta}], \tag{3.17a}$$

$$(1-\beta\eta)^{-1}\Psi_1+\partial_r\Psi_1=(1-m)W_{if}\eta+3SW_{if}[w^{(0)}|_{y=-\eta}]. \tag{3.17b}$$

When m is asymptotically greater than β: $m\gg\beta$ and thus $W_{if}=2m^{-1}\beta+O(\beta^2)$, for $S\sim1$ we can estimate magnitudes of boundary values at $r=1-\beta\eta$ as

$$\partial_z\Psi_1=O(\beta^2m^{-1}),\quad \Psi_1+\partial_r\Psi_1=O(\beta m^{-1}). \tag{3.18}$$

Therefore the last term in (3.11) is of the order of βm^{-1} at most, and for sufficiently strong surface tension the effect of interfacial shear can be neglected in the leading-order equation which takes the closed form

$$\eta_t+\eta\eta_z+S\{(1+\eta)^3(\eta_z+\eta_{zzz})\}_z=0, \tag{3.19}$$

and recall that (3.11) and (3.19) are written in a reference frame moving with the speed of unperturbed interface (one in the rescaled non-dimensional units).

Inference on negligibility of coupling with the core for $S\sim1$, based on (3.18), remains valid for $m\gg\beta$ in the case when (small) perturbations of the core flow can be described by the Orr–Sommerfeld equation with the Reynolds number $\mathbb{R}_1$ of order one.

In a laboratory reference frame connected with tube walls, it is useful to rewrite (3.19) in terms of the full dimensionless thickness $h = 1+\eta$

$$h_t + hh_z + S\{h^3(h_z + h_{zzz})\}_z = 0. \tag{3.20}$$

We note that only positive solutions $h = O(1)$ are asymptotically consistent.

The weakly nonlinear limit when $S \ll 1$, and intermediate cases when both the nonlinearity and the interfacial shear are essential, will be discussed in §6.

Other long-wave evolution equations of film flows have a form close to (3.20): the Benney equation for film on an inclined plane (Benney 1966; Gjevik 1970; Pumir, Manneville & Pomeau 1983) and equation of thin film flowing down a fibre (Frenkel 1992; Kerchman & Frenkel 1994). The latter differs from the decoupled CAFF equation (3.20) only by nonlinearity in the convective term

$$h_t + 2h^2h_z + S_g\{h^3(h_z + h_{zzz})\}_z = 0. \tag{3.21}$$

Hammond (1983) studied nonlinear adjustment of a thin film within capillary in the absence of imposed flow and obtained equation

$$h_\tau + 3^{-1}\{h^3(h_z + h_{zzz})\}_z = 0, \tag{3.22}$$

which can be considered as a limiting case of (3.20) when parameter S is very large (after rescaling the latter to the same viscocapillary time $\tau = 3St$). We show below that the long-time behaviour of solutions to (3.20) in the limit $S \gg 1$ differs, however, from that for (3.22). Aul (1989) derived an equation equivalent to (3.19) as a generalization of the Hammond one, in the form

$$h_\tau + W(h-1)h_z + 3^{-1}\{h^3(h_z + h_{zzz})\}_z = 0, \tag{3.23}$$

where his control parameter $W = 1/(3S)$.

To solve (3.23), Aul (1989) used a method of lines by replacing spatial derivatives with central finite-differences, and integrating with respect to time the resulting nonlinear system of coupled ordinary differential equations. His limited solutions involved only short-time simulations of the monochromatic fastest growing disturbances on spatial intervals of length $L_0 = 2\pi\sqrt{2}$ and $3L_0$ (with one and three waveforms respectively), and showed their linear growth in time as standing waves in the reference frame of the interface. (That is true only for the very short initial stage.) We have repeated some of the computations by Aul using the pseudospectral method with the controlled global error $\lesssim 10^{-6}$ (it was evaluated by doubling the number of gridpoints and estimating the truncation errors, see §4 and Kerchman & Frenkel 1994 for details). Our computations detected serious discrepancies with the results in Aul (1989), even by the order of magnitude. Specifically, in the case of sufficiently strong imposed flow ($S = 0.033$–0.06) Aul's results (for his parameter $W > 4$) indicated 'halving of the wavelength' and dominance of the second harmonic in the wave profiles with amplitudes $\eta > 0.5$. Actual magnitudes in our simulations for the same data were far smaller ($\eta_{max} < 3S$) in this range of control parameter, and with less significant higher harmonics, see figure 1(*a*) for the same case as in figure 2.10 of Aul (1989): $W = 10.0$ (our $S = 0.033$). Only small-amplitude interfacial perturbations have been observed for large W (small S) in laboratory experiments by Aul (1989), and also in our simulations of extended systems (see §§4 and 6). Figure 1(*b*) for $S = 0.833$ shows the development of the three-lobe system from initial disturbances with the middle wave of larger amplitude than the other two (corresponds to the Aul case for $W = 0.4$ in his figure 2.17). Evolution differs from that predicted in computations by Aul: a 'mini-train' of saturating pulses emerges and it is moving slower than the unperturbed

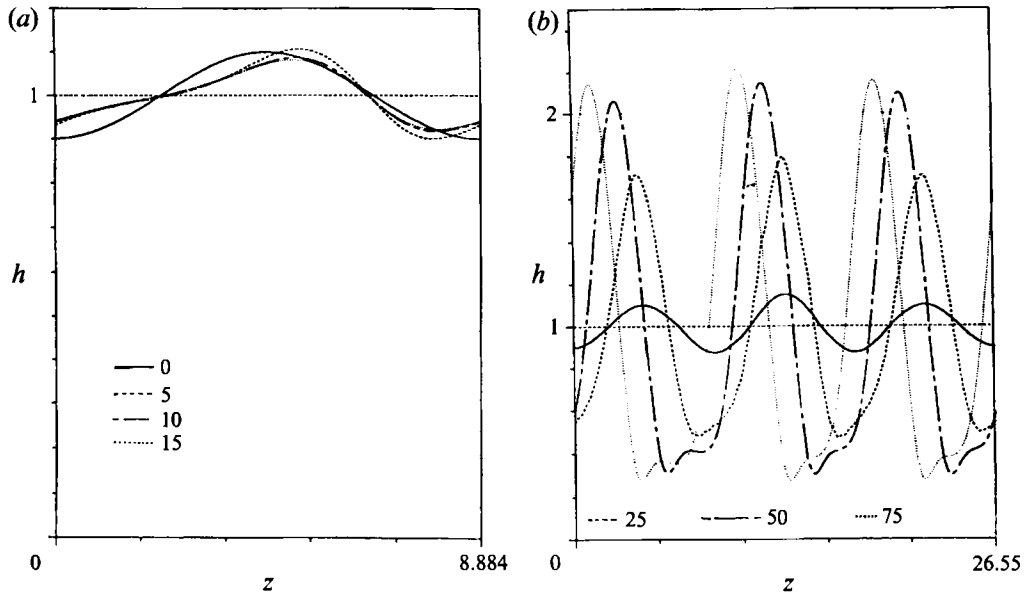

FIGURE 1. Evolution governed by (3.19) and (3.23) with the same parameters and initial conditions as in Aul (1989): (*a*) $S = 0.0333$ ($W = 10$) and monochromatic initial conditions on $0 \leqslant z \leqslant L_0 = 2\pi\sqrt{2}$ (compare with figure 2.10 in the work cited); (*b*) three-lobe evolution for $S = 0.833$ ($W = 0.4$) on $0 \leqslant z \leqslant L = 3L_0$ with initial disturbances $\eta = -0.1\cos(2\pi z/L) - 0.05\cos(6\pi z/L)$, corresponds to figure 2.17. Dashed line $h = 1$ indicates the unperturbed interface. Numbers show time τ for (3.23), respective times for (3.19) are $t = \tau/(3S)$.

interface. No droplet-like formations between major lobes (claimed to be similar to the satellite lobes in simulations of Hammond equation) were observed either here or in our simulations of spatially extended systems for $S < 1$. (They do appear as a temporary pattern for larger S which correspond to the conditions of those experiments by Aul & Olbricht (1990) where the secondary lobes were observed, see figure 8 and remarks in the next section.) Errors in computations by Aul might be due to inadequate approximation of the convective term in the method of lines and insufficient resolution of finite-difference substitutes to the high-order derivatives.

The assumptions used in the derivation of (3.11) and (3.20) are satisfactorily realized for the conditions in which water displaces oil in the capillary pores ($m > 1$) with reasonable capillary numbers $\mathbb{C} \ll 1$. Specifically, in the relevant experiments by Aul & Olbricht (1990) (see also Aul 1989), the parameters are: the tube radius $\bar{R}_2 = 27$ μm, the initial thickness ratio 0.03–0.09, and the viscosity ratio for the model wetting fluids $m = 19; 80; 173$. The Reynolds numbers in the core were small enough: $\mathbb{R}_1 < 0.04$. The capillary number $\mathbb{C} = \bar{\mu}_1 \bar{V}/\bar{\sigma}$ varied over the range 0.002–0.04 (here $\bar{V} \approx \frac{1}{2}\bar{W}_c$ is the average velocity in the core), and the values of our parameter S were in the range $2.2 \geqslant S \geqslant 0.1$. The film liquid gathered into lobe-like structures owing to interfacial instability, and further development resulted in the formation of a lens and pinch-off of the water core, except in the regime when Aul's parameter W was greater than 2 (our $S < 0.16$). In the latter case, the undulating interface with asymmetric lobes continued to propagate downstream, keeping the annular film configuration intact.

The small-box-confined simulations do not reveal all the fundamental pecularities of the real extended systems (Hyman, Nicolaenko & Zaleski 1986; Cross & Hohenberg 1993; Kerchman & Frenkel 1994). Detailed study in §§4–6 demonstrates a wealth of

complicated dynamics in interfacial evolution governed by (3.20) and (3.11) which strictly depends on S (and other parameters). Our numerical simulation also shows phenomena observed in experiments by Aul & Olbricht.

We can also rewrite (3.20) in the original dimensional variables

$$\bar{h}_{\bar{t}}+\frac{\bar{W}_{tf}}{\bar{h}_0}\bar{h}\bar{h}_{\bar{z}}+\frac{2}{3}\frac{\bar{\sigma}\bar{h}_0}{\bar{\mu}_2}\{\bar{h}^3(\bar{R}_2^{-2}\bar{h}_{\bar{z}}+\bar{h}_{\bar{z}\bar{z}\bar{z}})\}_{\bar{z}}=0. \tag{3.24}$$

Here $\bar{h}_0=\beta\bar{R}_2$ is the mean film thickness over the entire spatial interval in consideration, and $\bar{W}_{tf}=\frac{1}{2}\bar{F}\bar{R}_2\bar{h}_0/\bar{\mu}_2$ is the respective unperturbed interfacial velocity. We assume these dimensional global parameters to be fixed in the course of the evolution, although (3.24) remains valid in a more general case when the total volume of annular film varies, as in certain experiments by Aul & Olbricht (1990), provided that the variation is slow enough.

Within a very long system with steady influx and outflow the periodic boundary conditions on extended intervals appear to be natural, and they are set in most numerical solutions of the film evolution equations. It should be noted, however, that even with fixed parameters, large-amplitude interfacial evolution can lead to the rise of lengthy subsystems which are characterized by a different local mean thickness, see below. Equation (3.24) allows us to interpret these large-scale inhomogeneities via internal renormalization.

4. Long-term behaviour of extended systems: chaos, pulse trains, and coalescence

We integrated evolution equations in the form (3.19) and (3.20) with periodic boundary conditions on extended intervals $0\leqslant z\leqslant 2\pi q$ using the pseudospectral Fourier method and a simple predictor–corrector scheme for stepping in time (Euler predictor with the trapezoidal corrector step were used in most computations.) In order to avoid aliasing, the higher $\frac{3}{5}$ of Fourier harmonics of h were smoothed to zero (for more details on numerical technique see Kerchman & Frenkel (1994) where equation (3.21) with the same quartic nonlinearity is considered.) With tough restrictions on the time-step imposed by the spectral stability condition, the spatial resolution was more a concern than the time-step errors. Accuracy of the spectral approximation was evaluated by magnitudes of the truncated modes, and the results were verified by doubling the number of grid points where necessary. We studied long-time evolution for values of S from 0.01 to 5. Parameter q was taken in the range $8\leqslant q\leqslant 25$ with the corresponding number of grid points from 256 to 1024. Thus, the systems considered are lengthy enough to accommodate a significant number of the fastest growing linearly unstable modes. The complex dynamics of evolving patterns strongly depend on the control parameter S. According to (3.11) and (3.20), the global mean film thickness has to be conserved, and this requirement, as well as the accuracy of computations (based on estimates of truncated harmonics), was thoroughly controlled.

As for initial conditions $h(z,0)$, we set them to two different types for the disturbances of the uniform film: (i) 'large-scale' disturbances, the sum of a small number of lower modes $A_k\cos(kz/q+m_k\pi/2)$, with $k=1,\ldots,6$ and either (all amplitudes) $A_k=0.02$ or $A_k=0.05$; and (ii) 'quasi-random' small disturbances which contained all active modes.

For very small values of $S<0.04$, the primary instability saturates with amplitudes of waves so small ($\eta<0.1$) that nonlinearity in the surface-tension-dependent terms of (3.19) is insignificant and evolution is very close to that in the weakly nonlinear case

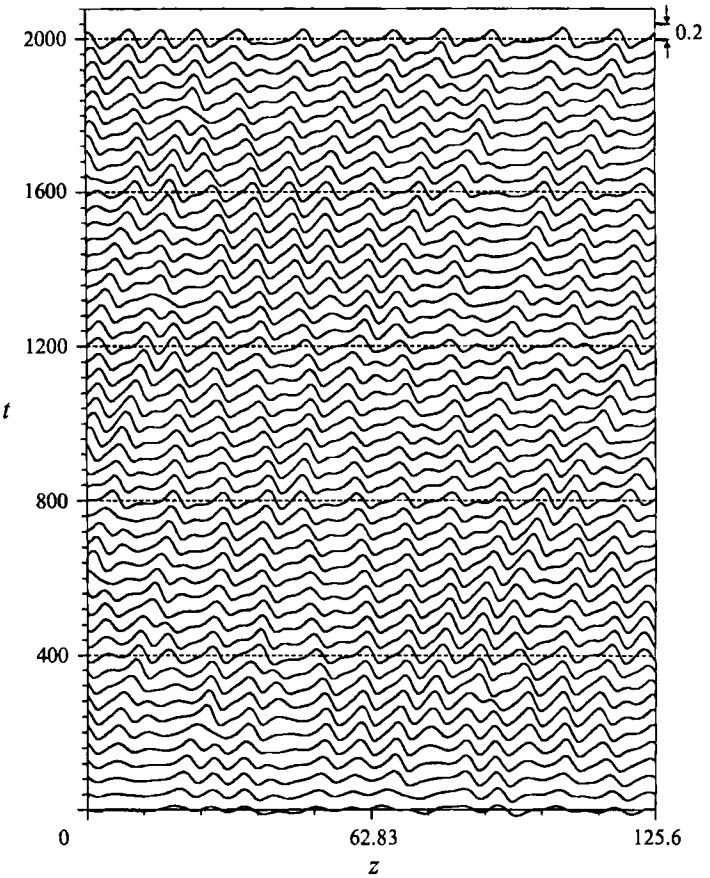

FIGURE 2. Quasi-chaotic evolution governed by (3.19) with periodic conditions on $0 \leqslant z \leqslant 2\pi q$ ($q = 20.0$) for $S = 0.05$. Interfacial profiles are shown successively shifted at time intervals $\Delta t = 40$, the amplitude scale is given at the right-hand side. Note that the dashed auxiliary axes here and in some figures below indicate the zero level of the ordinate variable – either η or h – for the selected snapshots.

governed by the Kuramoto–Sivashinsky (KS) equation. Solutions exhibit spatio-temporal chaotic behaviour with a finite-dimensional attractor as inertial manifold as described in numerous studies, see Hyman *et al.* (1986), Constantin *et al.* (1989), Collet *et al.* (1993), Cross & Hohenberg (1993). We consider this limit and related cases when the core dynamics becomes pertinent in §6.

For larger values of S, in the course of development of the fastest growing modes, initially a wavy regime is generated with $M_q = [q/\sqrt{2}]$ major peaks (see Iooss & Rossi (1989); Kerchman & Frenkel (1994) for similar situations). The timescale for an early stage of development is due to capillary instability of the dimensionless magnitude S^{-1} according to linearized analysis of the unstable growth. The actual process of pattern formation and evolution depends on essentially nonlinear effects which introduce different characteristic times for the mature stage (and additional lengthscales as well). Large-time evolution of the system for $0.05 \leqslant S < 0.08$ can be regarded as a quasi-chaotic defect-mediated dynamics of a cellular pattern (Coullet & Lega 1988; Cross & Hohenberg 1993). Figure 2 presents a series of snapshots at consecutive instants for $S = 0.05$. The train of disorderly moving N cells ($N < M_q$) is drifting slightly faster than the unperturbed interface, with complicated dynamics of waves of strictly

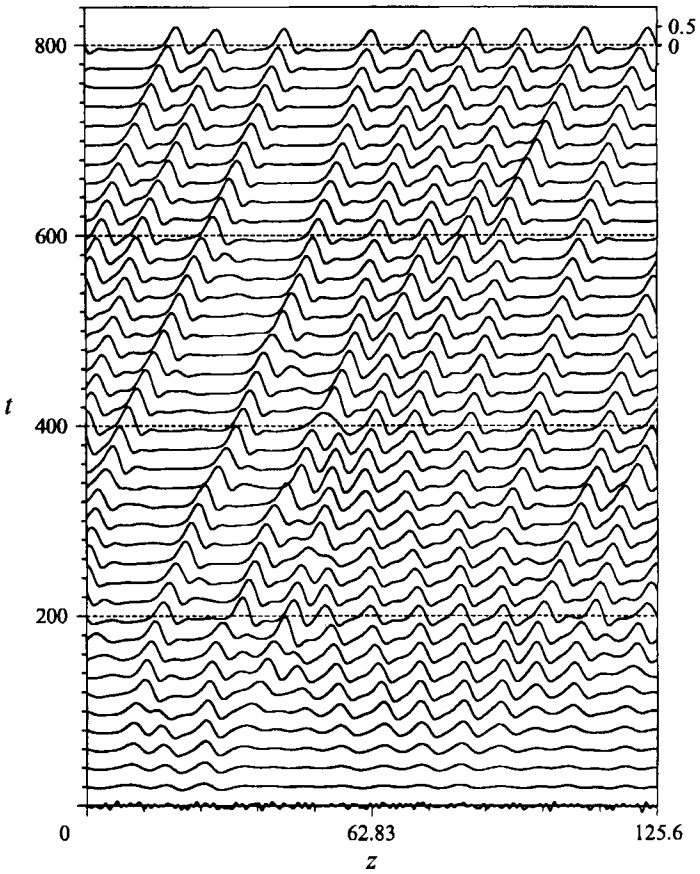

FIGURE 3. Development of a regular pulse train for $S = 0.125$ ($q = 20$, wave profiles at time intervals $\Delta t = 20$).

bounded amplitudes $\eta_{max} < 3S$. Observed phenomena include quasi-elastic collisions, cell mergers (period doubling), Eckhaus instability, nucleation of defects on cell boundaries, and intermittency.

For $S \geqslant 0.09$, development of the wavetrain from small-amplitude initial disturbances results in the formation of a more sparse pattern of coherent structures usually termed pulses (Cross & Hohenberg 1993; Kerchman & Frenkel 1994). Their number and disposition of major humps sensitively depends on initial conditions. (Pulse-forming mergers of the underdeveloped waveforms are seen in figures 3–5.) Further evolution of the system can be described in terms of motion and interactions of these stable pulses propagating as a whole.

Thickness of flattened film in spans between humps is almost constant and depends mainly on the value of S (and slightly on the 'size' of pulses). Figure 6 presents cumulative data on the 'substrate layer' thickness h_s versus S acquired from computer simulations for various initial conditions. Individual isolated pulses can be identified very closely with the spatially periodic travelling waves $h = h(z - Vt)$ to (3.20) for the different cell-lengths $2\pi\lambda$. These one-hump basic solutions (which for $\lambda > 1.2$ correspond to the supercritically stable structures) play a fundamental role in the description of the large-time behaviour and understanding of various interfacial interactions. We discuss them in more detail in the next section.

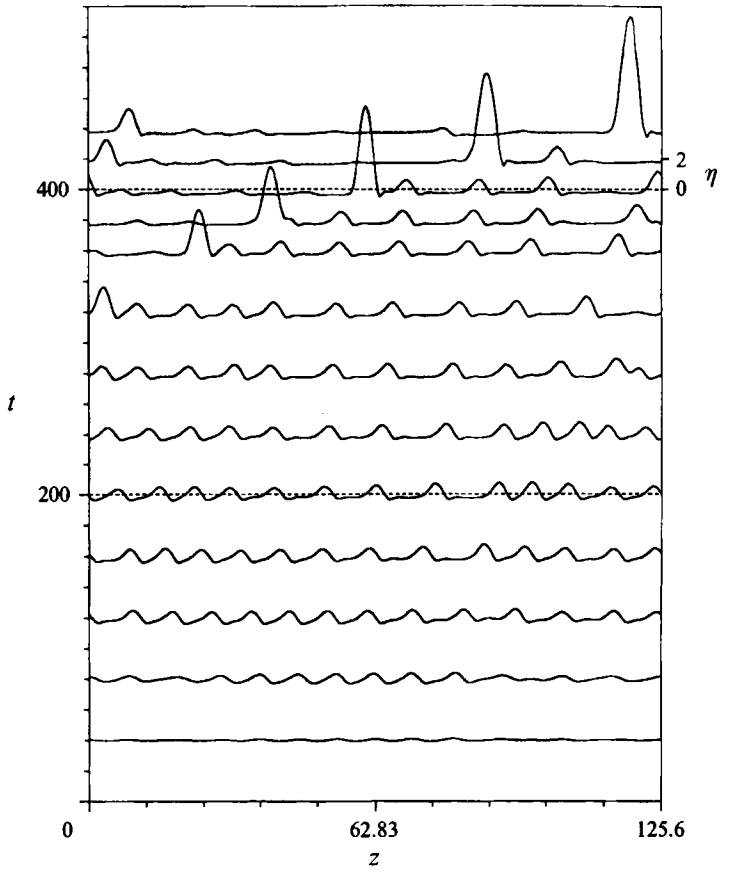

FIGURE 4. Evolution of the wavetrain for $S = 0.2$ ($q = 20$). The pulse which emerges near the left-hand edge at $t \cong 300$ travels faster and in passing absorbs smaller ones. The coalescences are not absolutely inelastic – a small droplet remains on the spot of collision.

When differences in sizes and velocities of the adjacent pulses are sufficiently small, their mutual interactions take place without merger (particle-like) and result in a slow 'quasi-elastic' exchange of amplitudes and velocities. For large times after a series of weak interactions the system tends to a steady propagation of identical pulses, as figure 3 shows for $S = 0.125$. That explains the tendency of lobe-like structures to equilibrate in size noticed by Aul (1989) in his experiment with our $S \approx 0.12$. This kind of behaviour with a steady attractor is typical in the narrow window $0.09 < S < 0.15$, so the primary saturated pattern is kept intact. It might happen when values of S are larger but only for a meagre class of the regular initial conditions which evolve into a system of nearly equal pulses.

For $0.15 \leqslant S < 1.0$, the pulse train evolution is dominated by another phenomenon: collision of two structures, one of which is larger enough than the other, brings about their coalescence. The enlarged pulse travels faster, and when it catches up with smaller ones swallows them up, leaving an elongated section of thinned flattened film behind, as figures 4 and 5(*a*) show for $S = 0.2$ and $S = 0.8$, respectively. Figure 5(*b*) shows that the hump height (and velocity) undergoes only insignificant slow variations between mergers, but grows abruptly in the short acts of coalescence. Such an avalanche-like fusion cascade leads to the formation of a tall 'solitary' structure with the local film

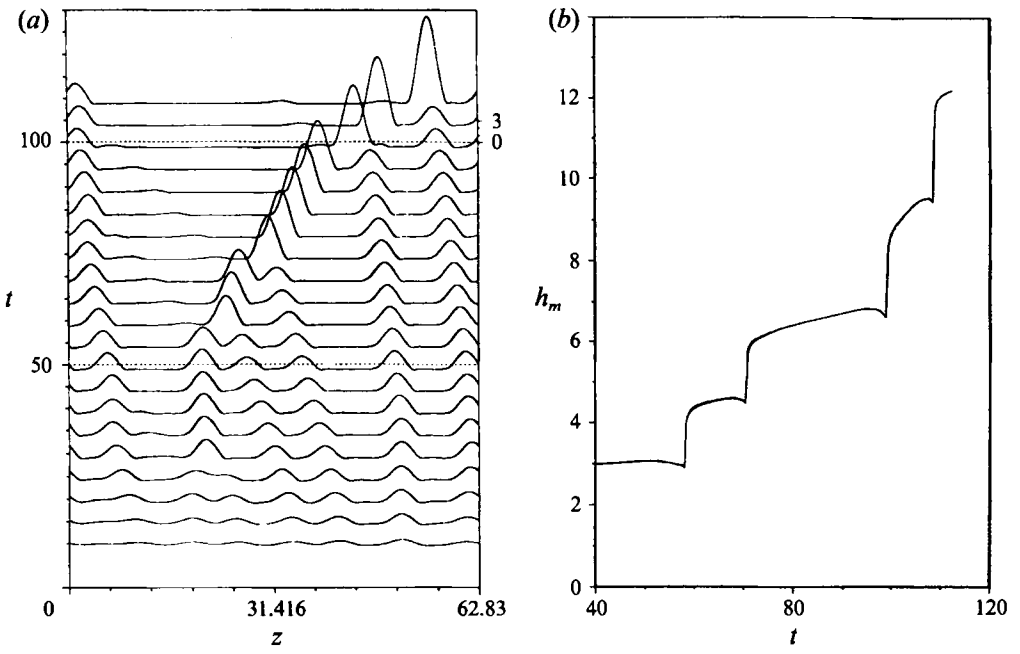

FIGURE 5. (*a*) Coalescence cascade for $S = 0.8$ ($q = 10.0$). (*b*) Time dependence of the peak's height h_m for a growing pulse.

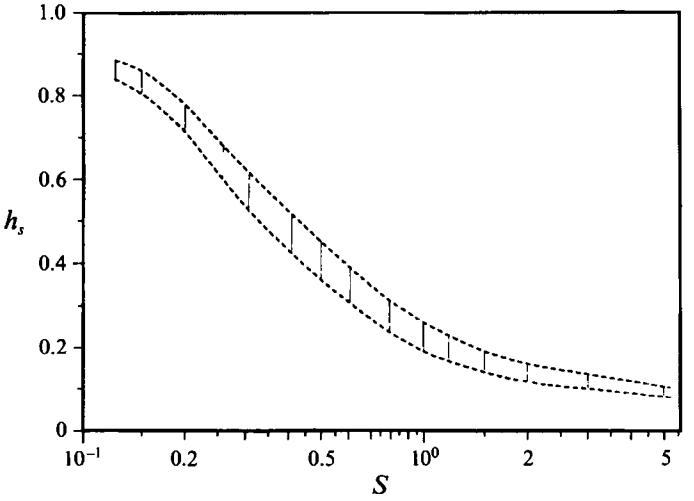

FIGURE 6. Variation of the substrate layer thickness h_s (between the dashed curves). Each vertical segment shows the range of thinning for the corresponding value of S (as a summary of computational experiments).

thickness several times larger than the average one. For very lengthy systems coalescences start in different spots simultaneously, and the large 'predatory' pulses saturate when no film substance to absorb is available (in excess to h_s). A similar scenario with consecutive acts of swallowing was observed in experiments on films down a fibre by Quéré (1990), and appeared in simulations of the relevant evolution equation (3.21) by Kerchman & Frenkel (1994) (who ascertained it to be related to the

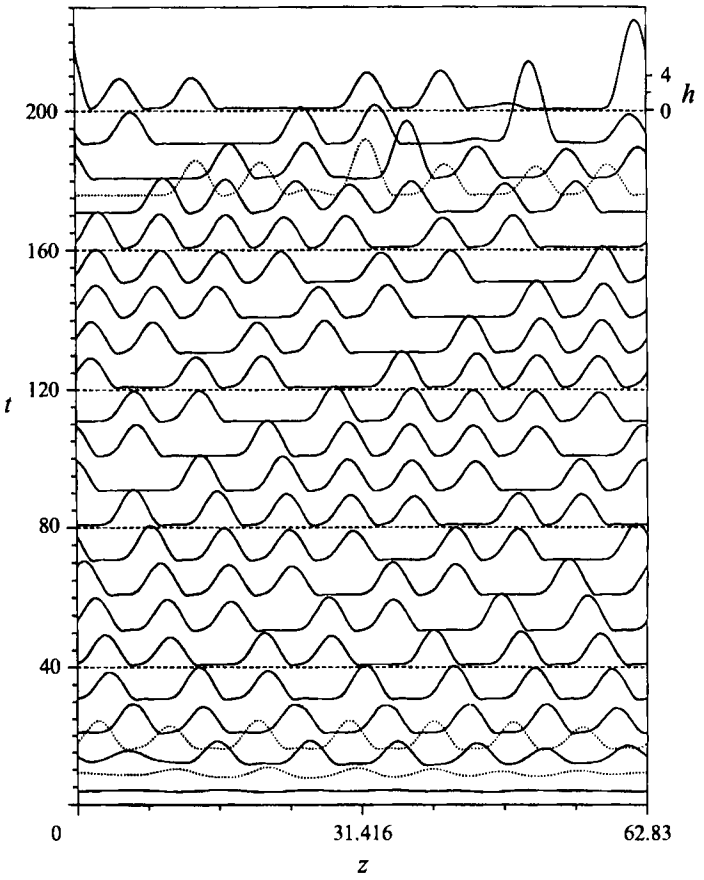

FIGURE 7. Simulation of (3.19) for $S = 1.5$ ($q = 10$). Profiles of the full thickness $h = 1 + \eta$ are plotted in a reference frame of the unperturbed interface. Coalescence at $t \cong 175$ (dotted profile) occurs as a result of the multi-pulse interaction.

deep inelasticity of the pulse interactions.) Liu & Gollub (1994) observed absorption of small waves by a larger one and formation of 'solitary' pulses in a film flowing down an inclined plane. In our problem, considerable local thickening of the annular film in the collar-like structures can cause loss of stability and the lens formation as in experiments by Aul & Olbricht (1990), see also the next section.

Figure 7 shows that coalescences may occur for $S \geqslant 1$ as a result of long-term group interactions. The mergers are less likely to happen for $S > 2$ (figure 8). In this range of parameter the film structure is highly inhomogeneous, with its volume mainly collected in slowly moving lobe-like structures, usually crowded in groups (hump packets), and very thin film in lengthy spans between them. This thinning limits the film liquid influx to a lobe in the same way as for Hammond's equation. The characteristic times for a flattened 'substrate' are far greater than the other timescales of the system. Thus, the secondary processes in lengthy spans of this thinned film, of dimensional thickness $\bar{h}_0' = h_s \bar{h}_0$, which can be treated via proper renormalization of (3.24) with the local parameter $S' \approx Sh_s^2 < 0.1$, are of negligible magnitude and do not influence major humps and their interactions. The mean thickness calculated over the long hump packets in figures 7 and 8 is 1.4–1.6 of the global mean, and thus the effective magnitude S'' of the control parameter there is actually 2–2.5 times greater than the

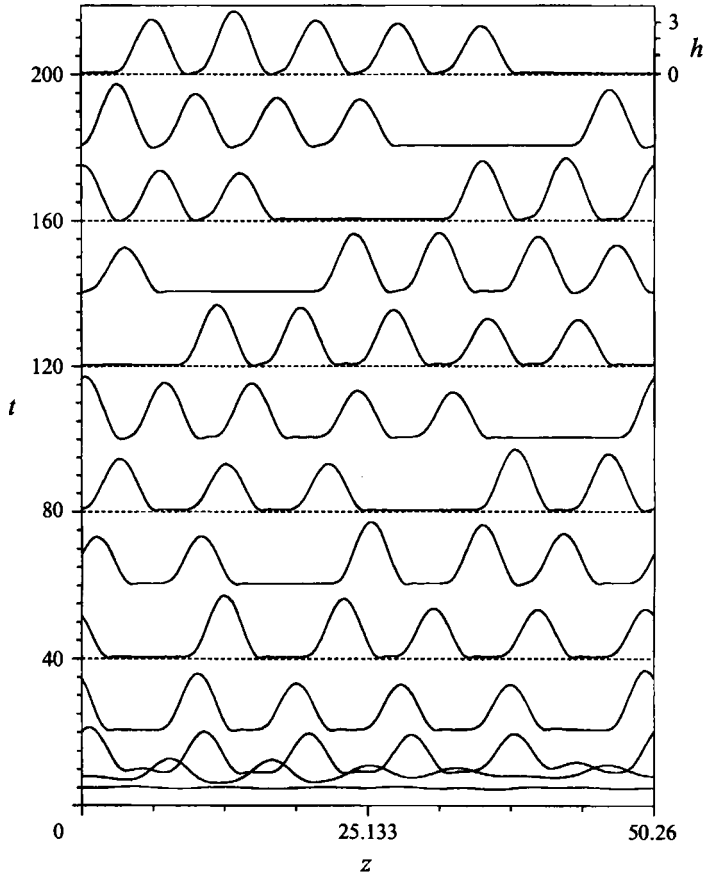

FIGURE 8. Train of lobes in the conditions of long-time group interactions and no mergers for $S = 3.0$ ($q = 8$, simulation of (3.20) in a laboratory reference frame). The film in long spans is thinned to $h_s = 0.09$–0.1, and the minimum thickness in troughs $h_{min} = 0.01$–0.015.

nominal one. The minimum thickness of the film (in 'troughs' between the interacting humps) can be extremely small for $S > 2$: dimensionless $h_{min} < 10^{-2}$. For the reasonable film thickness in narrow capillaries $\bar{h}_0 = (1\text{–}10)$ μm, the van der Waals forces become significant at $\bar{h}_{min} \sim 0.1$ μm (Aul & Olbricht 1990), and this can cause rupture of the film. Even if the film neither rearranges into lenses owing to local thickening nor ruptures because of thinning, this extremely non-uniform configuration should not be regarded as a regular CAFF – it is, rather, slow pushing of coagulated lobe clusters (in particular, magnitudes of the flux along the film vary by several orders.) Large-time behaviour is different from the limiting case ($S = \infty$) of the Hammond equation (3.22) in which the long-term evolution results in partitioning of the film into a number of separate static lobes and the small satellite lobes (droplets) between them (Hammond 1983). No droplets will survive under an arbitrary weak imposed flow, they are eventually absorbed by the moving lobes as in figure 8. It takes, however, a considerably longer time than the duration of experiments by Aul & Olbricht (1990) where only an early stage of satellite lobe formation was observed, similar to that for times $20 \leqslant t \leqslant 40$ in figures 7 and 8.

5. Steady pulses and their interactions

We consider evolution equation in the form (3.20) and are seeking uniformly translating pulse-like solutions $h = H(Z)$, $Z = z - Vt$. They satisfy an ordinary differential equation which can be integrated to yield a third-order equation

$$SH^3(H''' + H') - VH + \tfrac{1}{2}H^2 = C. \tag{5.1}$$

Solitary-wave solutions satisfying the conditions $H = 1$, $H' = H'' = H''' = 0$ at infinity have been investigated for the dispersive–dissipative equation in Kawahara & Toh (1988), Chang, Demekhin & Kopelevich (1993), and for the Benney equation by Pumir *et al.* (1983). In the case of the film-down-fibre equation (3.21), Kalliadasis & Chang (1994) argued that solitary waves do not exist for sufficiently larger values of the control parameter $S_g > 1$. These soliton-like structures for (3.20) are subjected to Rayleigh instability at their flat 'wings' far from the peak and do represent any meaningful asymptotics to an initial-value problem, and the same is true for the above-mentioned equations. Amick & Toland (1992) rigorously proved non-existence of true solitary waves for an equation close to (5.1), and revealed the complicated nature of trajectories homoclinic to a set of periodic orbits in a neighbourhood of equilibrium, i.e. to a state with quasi-periodic ripples at infinity. As for other dissipative systems that are convectively unstable, and similarly to the equation (3.21) that we studied before (Kerchman & Frenkel 1994), of special interest are spatially-periodic travelling waves to (3.20) with the appropriate periodicity lengths $2\pi\lambda$ ($\lambda_*(S) > \lambda > 1.2$) which reflect a cellular pattern of evolving pulse trains. (In the nonlinear analysis of the saturation of monochromatic disturbances for the Benney equation by Lin (1969), Gjevik (1970), and Joo & Davis (1992) similar structures are termed super-critically stable permanent waves.) We can choose integration constant C in (5.1) as $C = \frac{1}{2}H_s^2 - VH_s$, where $H_s < 1$ is the thickness in the point outside the crest where $H''' + H' = 0$ (obviously $H_s(S, \lambda)$ are in the range of substrate thicknesses, $h_s(S)$ appeared in the simulations of extended systems). The steady pulse solutions were constructed with high accuracy by an iterative spectral method. We started by solving (3.20) with periodic conditions on $0 \leqslant z \leqslant 2\pi\lambda$ and the suitable 'single-hump' initial conditions, and integrated the equation until the development settled to a quasi-steady propagation (by setting starting state via continuation in λ and S it was reached in a reasonable time.) This solution $H^{(1)}(Z)$, and the corresponding values of the pulse speed $V^{(1)}$ and substrate thickness $H_s^{(1)}$ were used as a first approximation. We then improved it on an N-grid $Z_l = 2\pi\lambda l/N$ by means of relaxation

$$H_l^{(j+1)} = H_l^{(j)} + \vartheta\,\Delta H_l (l = 0, \ldots, N-1), \quad V^{(j+1)} = V^{(j)} + \vartheta\,\Delta V, \tag{5.2}$$

with $\vartheta = 0.5$–0.7. Here ΔV and the Fourier coefficients of the increment $\{Y_k\} = \mathscr{F}[\Delta H]$ for a given periodicity $2\pi\lambda$ are obtained from a spectral form of the Newton–Raphson step in finding the solution to (5.1) (properly truncated to ensure dealiasing)

$$\sum_{k=-\frac{1}{4}N}^{\frac{1}{4}N} \{\mathrm{i}B_{n-k}(\lambda k - \lambda^3 k^3) + D_{n-k}\}\, Y_k - A_n\,\Delta V = G_n, \tag{5.3}$$

$$n = -\tfrac{1}{4}N, \ldots, \tfrac{1}{4}N; \quad Y_0 = 0, \quad Y_{-k} = Y_k^*,$$

where the coefficients and right-hand sides are the discrete Fourier transforms computed with the previous approximation $H = H^{(j)}$

$$\left.\begin{aligned} &\{A_k\} = \mathscr{F}[H], \quad \{B_k\} = \mathscr{F}[S(H)^3], \\ &\{D_k\} = \mathscr{F}[3S(H)^2(H''' + H') + H - V^{(j)}], \quad \{G_k\} = \mathscr{F}[C^{(j)} - \tfrac{1}{2}(H)^2]. \end{aligned}\right\} \tag{5.4}$$

For the convergence with the acceptable approximation errors 10^{-5} we typically used $N = 256$.

Pulse solutions for the cell-length 4π ($\lambda = 2$) and different values of S are shown in figure 9. Figure 10 illustrates dependence on the cell-length. The hump width at the unperturbed level $h = 1$ is virtually independent of both S and λ: $\Delta z \approx 1.5\pi$ – the same as appeared for all pulses in simulations of extended systems. Thus the tube radius indeed continues to serve as a major axial lengthscale in the developed stage of evolution. In the front of the crest the film thickness undergoes damped undulations with a substantial first depression. This profile reflects the analytical structure of a dynamical system associated with (5.1) near the homoclinic intersection of Shilnikov's saddle-focus type at $\{H = H_s,\ H' = 0,\ H'' = 0\}$ in the same way as for systems studied by Pumir *et al.* (1983), and Kerchman & Frenkel (1994). Indeed, we can rewrite (5.1) as a three-dimensional system with a tangent form in the origin

$$\frac{\mathrm{d}U}{\mathrm{d}Z} = \begin{pmatrix} 0 & 1 & 0 \\ 0 & 0 & 1 \\ \dfrac{V-H_s}{SH_s^3} & -1 & 0 \end{pmatrix} U, \tag{5.5}$$

where $U_1 = H - H_s$, $U_2 = H'$, $U_3 = H''$. Cubic equation for eigenvalues of the linearization matrix

$$\mu^3 + \mu - \frac{V-H_s}{SH_s^3} = 0, \tag{5.6}$$

has a real root μ_1 of the same sign as $V - H_s$ (positive in our case, that defines a one-dimensional unstable manifold) and a pair of complex conjugate eigenvalues $-\frac{1}{2}\mu_1 \pm \mathrm{i}\phi$. An infinite number of periodic orbits, including the constructed pulse solutions, do originate in the neighbourhood of points $\{H = H_s,\ H' = 0,\ H'' = 0\}$. However, the existence of an orbit homoclinic to the unperturbed state $\{H = 1,\ H' = H'' = 0\}$, which corresponds to a true solitary wave, is questionable even for small S.

Thickness $H_s(S, \lambda)$ slightly decreases with increasing λ. The maximum height of a stable pulse H_m is roughly proportional to λ as the cell-length increases, and the local thickness grows correspondingly (over the piece of the axial length 2π enclosing the hump).

The pulse speed $V(S, \lambda)$ increases very slow with λ, especially in the case of large $S \gg 1$ for which $V < 1$ (motion is retarded by an increased resistance along the thinned part of the film). The dependence differs from that for the travelling pulses to (3.21) studied previously by Kerchman & Frenkel (1994). This is manifested in mentioned differences of the long-time behaviour for $S > 2$.

For $\lambda > \Lambda^{(n)} \approx 2.8\pi n$ there exist l-hump travelling-wave solutions ($k = 1, \ldots, n$) which are different from the slightly perturbed mini-trains of primary solitary pulses (of cell-length λ/l each). The bifurcating stationary solutions are analogous to some multi-peak waves constructed for the Benney equation by Pumir *et al.* (1983) and for the dissipative–dispersive equation by Chang *et al.* (1993). Most of these second-kind sections are unstable or less stable than single-crest-in-cell solutions and their combinations, and are not considered here. We discovered, however, stable multi-peak structures in simulations of (3.11) (see figure 20).

The film velocity field in a reference frame moving with the steady pulse can be represented in terms of the (plane-type) stream function Ψ_2

$$W_2 + w_2 - \beta W_{if}(V-1) = \beta \partial_y \Psi_2, \quad u_2 = -\partial_z \Psi_2 \tag{5.7}$$

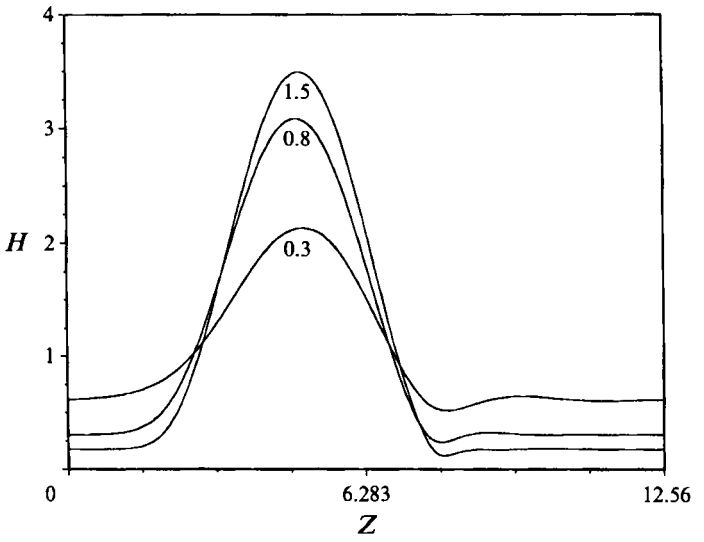

FIGURE 9. Steady pulse profiles (with the cell-length 4π, i.e. $\lambda = 2.0$) for different values of S (shown at the crests).

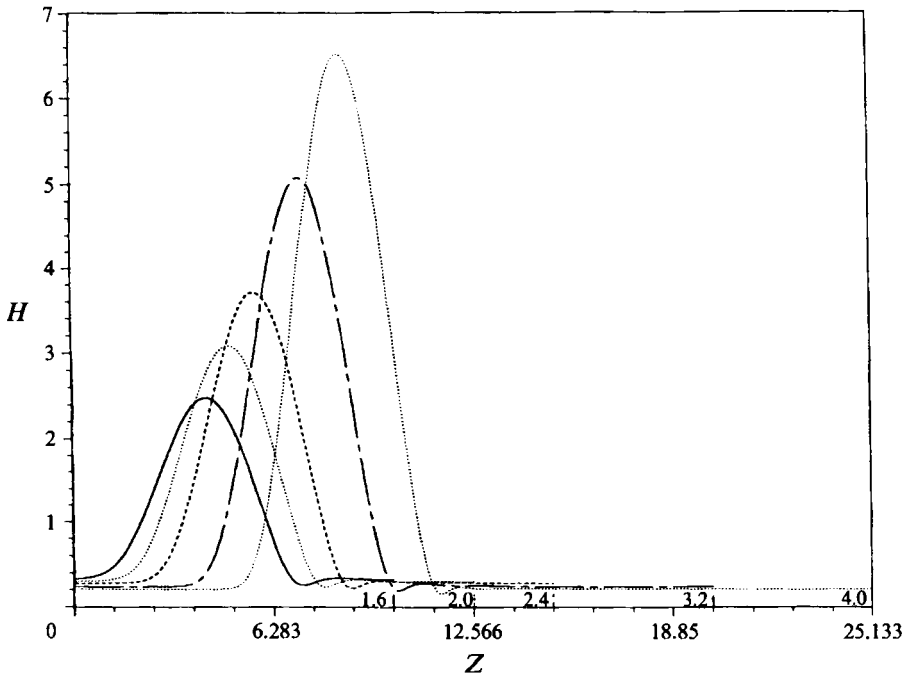

FIGURE 10. Pulse solutions with different spatial periods $2\pi\lambda$ for $S = 0.8$. Each short vertical line at the Z-axis indicates the end of the respective cell, and the value of λ is given next to it.

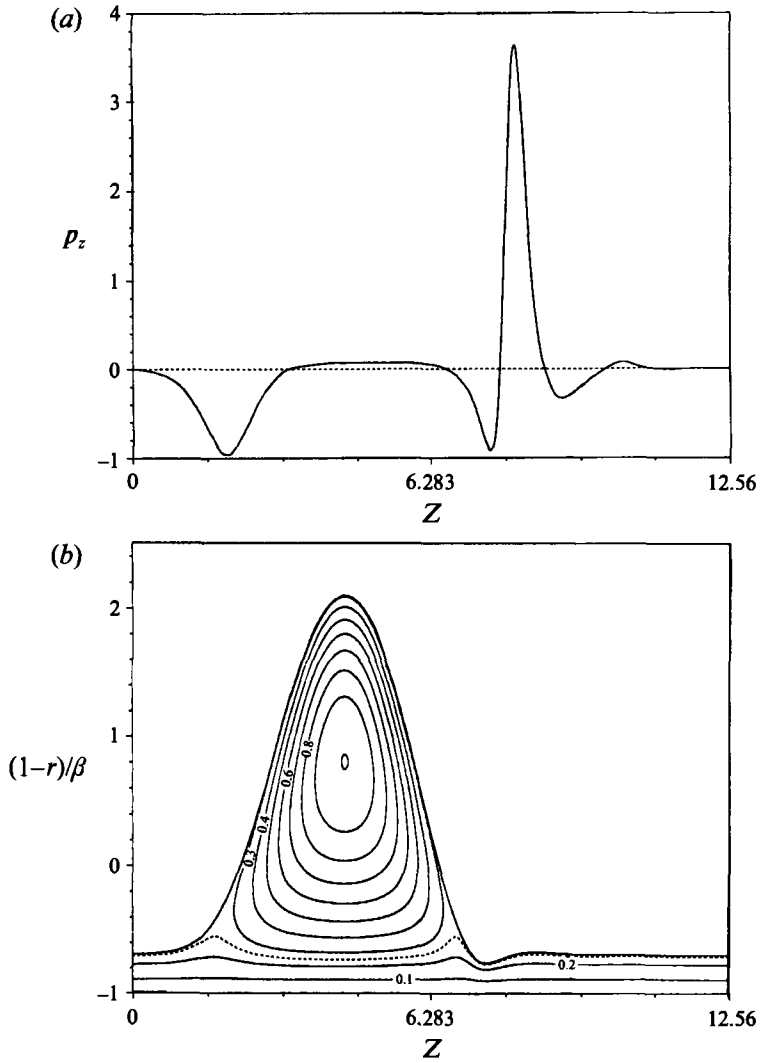

FIGURE 11. (*a*) Profile of the pressure gradient $p_z = -S(H_z + H_{zzz})$ along the travelling pulseform for $S = 0.8$ ($\lambda = 2.0$). (*b*) Steady streamline portrait for rescaled flow (5.7) and (5.8) in a cell moving with the speed $V(S, \lambda) = 0.99$. Dash curve correspond to the value 0.25 and is close to a separating streamline. Ordinate variable $(1-r)/\beta = -y$.

where according to (3.7) and (3.9)

$$\left.\begin{aligned} \frac{\Psi_2}{\beta W_{tf}} &= \tfrac{1}{2}(1-y^2)+(1-V)(y-1)+\tfrac{1}{2}p_z(y^3-2y+2-3\eta(1-y^2)), \\ p_z &= -S(\eta_z+\eta_{zzz}). \end{aligned}\right\} \tag{5.8}$$

Figure 11 shows the distribution of the perturbation pressure gradient p_z along the typical steady cell and the corresponding roll-wave streamline pattern (5.8). Capillary forces have high gradient in a narrow depression in front of the hump where thickness is minimal. It prevents the merger of two interacting unequal pulses as long as the

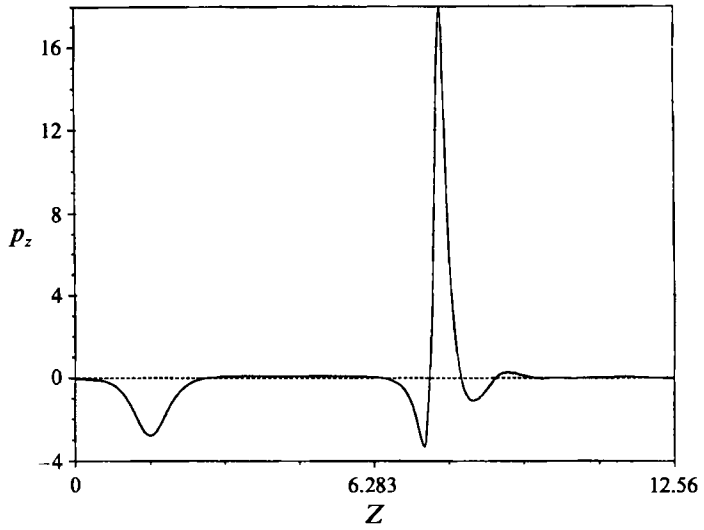

FIGURE 12. Pressure gradient along the steady pulse for $S = 1.5$ ($\lambda = 2.0$).

dynamics of relative motion is not strong enough to overcome this potential barrier (which can be very high for $S > 1$, see figure 12).

Interactions of 'free' pulses have local nature and in the simplest situations can be studied within a relatively short box with periodic conditions. Figure 13(*a*) shows the collision of two steady pulses from a family in figure 10 (for $S = 0.8$) with the cell-lengths $2\pi\lambda_1$ and $2\pi\lambda_2$ ($\lambda_1 = 2.4, \lambda_2 = 1.6$). It results in their coalescence similar to certain interactions in figure 5. In the instant of merger ($t \approx 20$) a structure of the double width l is formed with its local thickness ratio β_l (over the representative portion of the length $l \approx 3\pi$) about 2.5 times of the initial mean β_0 (see figure 13*a*, *b*). such a thickening does restrict further applicability of the simulation of figure 13 – which predicts the following formation of one larger pulse (and a far smaller residual droplet) – to very thin films, in this particular case with an initial thickness ratio $\beta_0 < 0.05$–0.06.

In the case of sufficiently wide annulus the large-amplitude thin-film equation (3.19), based on a quasi-flat velocity approximation (3.9) and the leading term of the Taylor expansion in the right-hand side of (2.9), may eventually become inconsistent with the essentially cylindrical geometry of the film. In particular, (3.9*a*) provides inadequate approximation for the perturbation pressure and its derivatives when $\beta\eta > 0.3$. Analysis of the capillary instability of sufficiently thick liquid collars was carried out by Everett & Haynes (1972) and Gauglitz & Radke (1988), and confirmed experimentally. These studies as well as numerical simulations by Johnson *et al.* (1991) and Newhouse & Pozrikidis (1992) – all of them with no imposed flow – indicated the transition of collar growth to a rapid rearrangement of the annular configuration into a double-meniscus bridge when the thickness ratio (over a section of the length $2\sqrt{2\pi}$) was greater than $\beta_{cr} = 0.1$–0.17. That explains the lens formation in the low-Reynolds-number experiments by Aul & Olbricht (1990) even for the initially thin annular films (β_0 ranging from 0.03 to 0.07) when values of our parameter S were greater than 0.16 – coalescence or just lobe-forming growth can increase local film volume to a supercritical level. (A rigorous higher-order analysis that supports the criterion of a local film thickness will be published elsewhere. It confirms that within its validity the leading-order equations provide a lower bound for the peak thickness, that can be

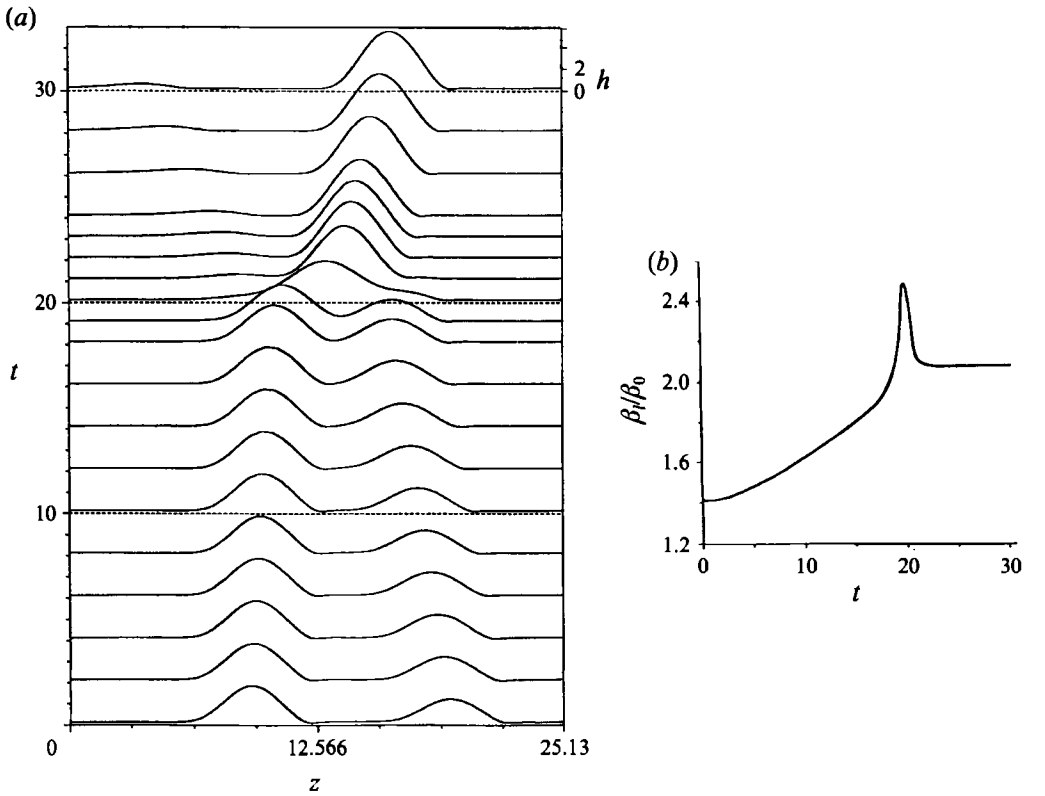

FIGURE 13. (*a*) Collision of two pulses for $S = 0.8$ within a small box ($q = \lambda_1 + \lambda_2 = 4.0$). (*b*) Time dependence of a local thickening factor β_1/β_0 (calculated as a volume of a section of the length 3π enclosing the larger peak).

understood from the cylindric volume conservation.) In the case of initially very thin films the critical thickness may be reached after a sequence of mergers as in figure 5, and remember that a sharp transition to the coalescence-dominated evolution occurs at $S_* \approx 0.15$. We do not consider here a slug flow regime which arises after infraction of integrity of the core by lenses of the wetting liquid and was observed by Aul & Olbricht (1990) (see approximate analysis in Bretherton 1961; Park & Homsy 1984; Schwartz, Princen & Kiss 1986; Georgiou *et al.* 1992).

Returning to the thin-film equations, we note that the dissipative system governed by (3.20) with periodic conditions on an extended spatial interval $(0, 2\pi q)$ for $S \geqslant 0.1$ has several stable branches of fixed points which correspond to the different number of identical 'solitary' pulses it can accommodate. As an example, for $q = 8.0$ and $S > 0.2$ this number can be from 1 to 6, with the respective cell-lengths $\lambda_k = q/k, k = 1, \ldots, 6$ (for $S = 0.8$ three 'generic' pulses from this family are seen in figure 10.) Steady k-pulse trains of different multiplicity have substantially distinct basins of attraction and unalike stability with respect to the finite-amplitude perturbations. (Certain combinations of the matching l-sections of the second kind – and the unsteady attractors – may exist as well.) The situation is typical also for other highly nonlinear interfacial equations: (3.21) studied in Kerchman & Frenkel (1994), the Benney equation (Joo & Davis 1992) – and pattern selection, in contrast to some weakly nonlinear problems (see e.g. Cross & Hohenberg 1993; Chang *et al.* 1993), cannot be based solely on the

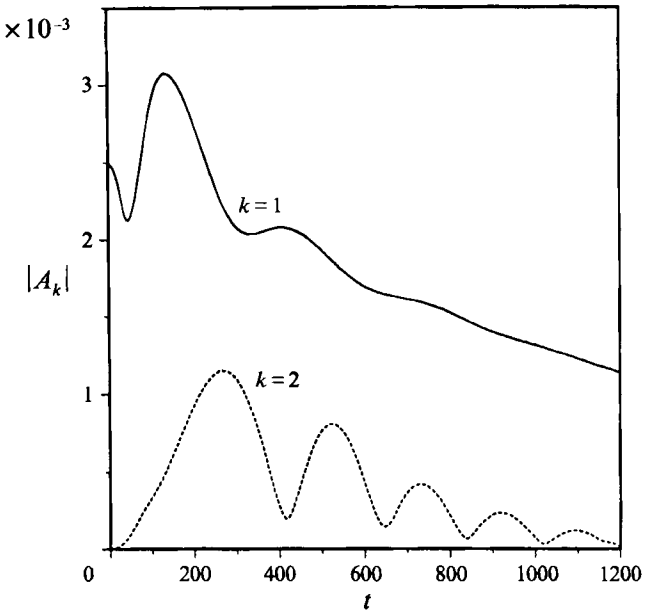

FIGURE 14. Time history of the primary ($k = 2$) and secondary ($k = 1$) subharmonics in the course of equilibration of a weakly modulated wavetrain for $S = 0.15$ ($q = 8$).

secondary 'infinitesimal' (in)stability. It was suggested for nonlinear waves in a film down an inclined plane (Joo & Davis 1992; Liu & Gollub 1994) that development of the spatially subharmonic instability in wavetrains may be responsible for the spatiotemporal irregularities or the formation of larger structures. We studied numerically secondary instabilities in the ideal patterns composed of identical steady pulses (5.1) and subjected to subharmonic disturbances. The initial conditions for the case in figure 14 correspond to four pulses with cell-length 4π ($\lambda = 2.0$) on the interval $(0, 2\pi q)$ where $q = 8\,(= 4\lambda_0)$, modulated by a long-wave disturbance $-0.005\cos(z/q)$. Evolution of the pulse train in this case of a near-threshold $S = 0.15$ is only slightly perturbed by the decaying weak interactions and tends to the equilibrated steady propagation. Figure 14 shows development of the lowest modes in a discrete Fourier representation

$$\eta(z,t) = \sum_{k=1}^{K} \{A_k(t)\exp(ikz/q) + A_k^*(t)\exp(-ikz/q)\}. \tag{5.9}$$

Magnitudes of both the primary subharmonics $|A_2|$ and secondary subharmonics $|A_1|$ are fading away at $t \to \infty$ (in similar computations for the Benney equation by Joo & Davis (1992) the undamped quasi-periodic in time or chaotic regimes were observed). Thus in the range of S where 'regular' pulse trains typically appeared in the long-time simulations in §4 ($0.09 \leqslant S \leqslant 0.15$) the steady pulse solutions turn out to be stable with respect to the small-amplitude subharmonic disturbances.

Evolution for $S = 0.3$ is presented in figure 15. A lattice of eight identical pulses of length 4π ($\lambda_0 = 2$) is superimposed by initial disturbance $-0.02\cos(z/q)$, $q = 16$. After a number of particle-like interactions in which both the primary subharmonics A_4 and secondary subharmonics A_2 are amplified, further development of the system leads to coalescence and the following cascade growth quite similar to figure 3. Thus a finite-amplitude subharmonic instability may indeed trigger mergers. The example shows

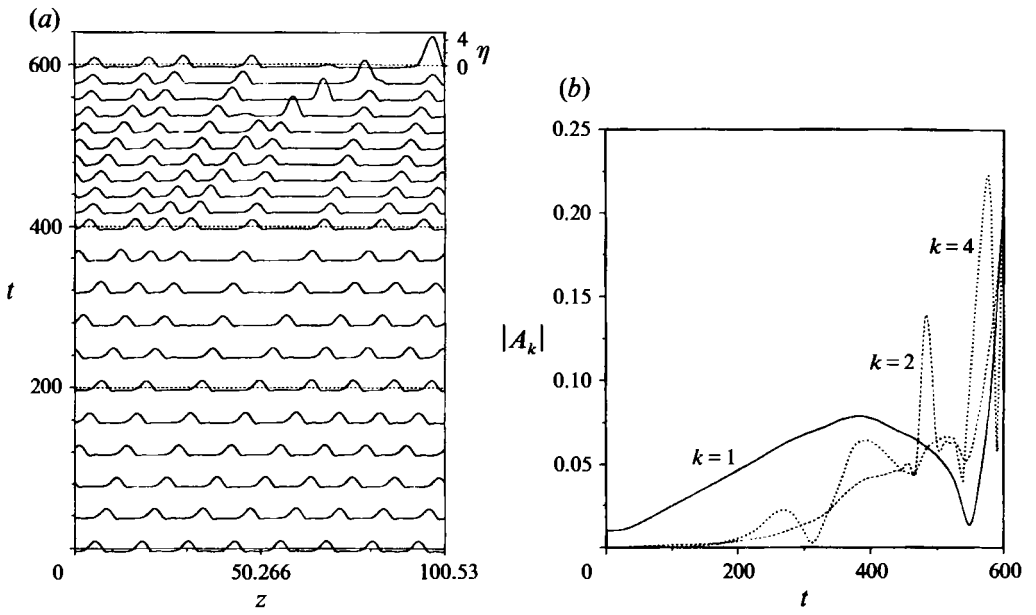

FIGURE 15. (*a*) Evolution of a long pulse train for $S = 0.3$ ($q = 16$). (*b*) Development of subharmonic modes. Coalescence may be initiated by the preceding growth of the secondary ($k = 2$) and primary ($k = 4$) subharmonics.

also that for almost all reasonable initial conditions the extended system is attracted to the same 1-cell state, as we observed in §4 for $0.2 \leqslant S < 1$ and $1 \ll q < \lambda_*(S)$ with the small-amplitude initial conditions. This is in sharp contrast with the prevalent behaviour in a subthreshold range of the parameter ($0.08 < S < 0.15$) when major basins of attraction are associated with the steady N-pulse trains ($\frac{1}{3}q < N < \frac{2}{3}q$).

6. Effects of the interfacial shear: weakly nonlinear limit and general case

For sufficiently small magnitudes of control parameter S (in particular, when $S = O(\beta^q)$ for some $q > \frac{1}{2}$) the amplitudes η in (3.11) are expected to be small as compared to the undisturbed film thickness (and this has been verified in our computations), that is $\eta_{max} \sim \delta \ll 1$. In the case of moderate viscosity, stratification perturbations of the core flow have their dominant order of $\Psi_1 = O(m^{-1}\beta\delta)$. Thus the last term in (3.11) may be neglected when $m^{-1}\beta = o(S)$ and the resulting small-amplitude evolution equation is a weakly nonlinear simplification of (3.19), the Kuramoto–Sivashinsky (KS) equation

$$\eta_t + \eta\eta_z + S(\eta_{zz} + \eta_{zzzz}) = 0, \tag{6.1}$$

which can be thrown into a standard form with all coefficients equal to one by means of $\eta = SX, t = \tau/S$ (and thus $\delta \sim S$).

Indeed, simulation in figure 16 of the highly nonlinear equation (3.19) for $S = 0.02$ demonstrates KS-like spatiotemporal chaos with strictly bounded amplitudes $\eta_{max} \leqslant 2.5S$ quite similar to that in Kawahara (1983) and Hohenberg & Shraiman (1989). Such a chaotic behaviour represents the dominant regime up to $S \approx 0.04$.

The interfacial shear in (3.11) cannot be ignored, however, when S is of the same (or higher) order in β as $(1-m)m^{-1}\beta$. Specifically, for $m > 1$ this means $q \gg 1$ (but

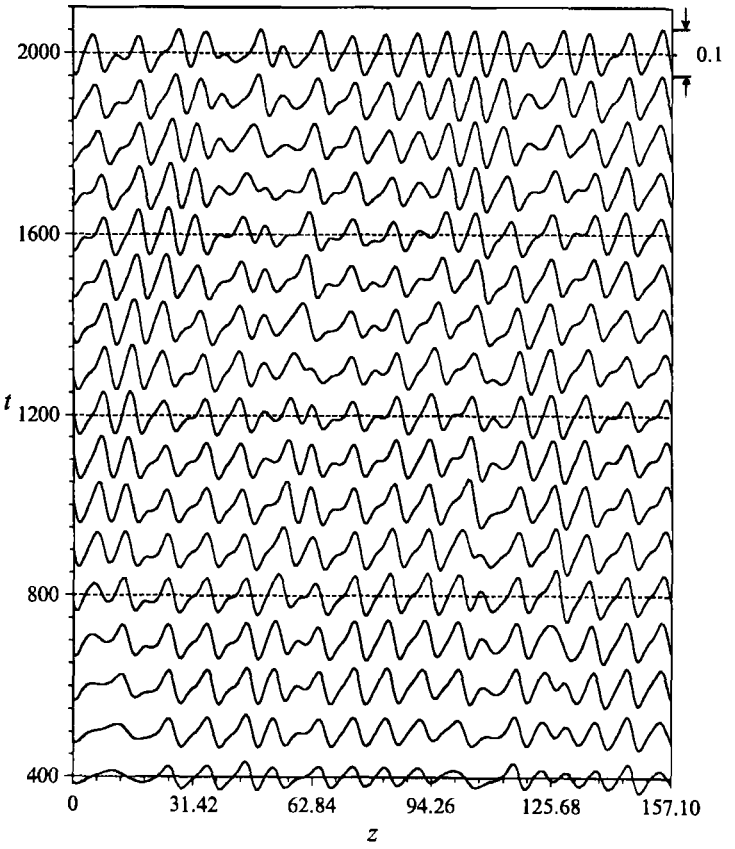

FIGURE 16. Spatiotemporal chaos in simulation of (3.19) for $S = 0.02$ ($q = 25$). Profiles are shown at time intervals $\Delta t = 100$.

$q < 2$). By omitting nonlinear factors $(1+\eta)^n$ in (3.11) we obtain its weakly nonlinear version, previously derived in Frenkel (1988) and Papageorgiou *et al.* (1990)

$$\eta_t + \eta\eta_z + S(\eta_{zz} + \eta_{zzzz}) - \frac{m+2\beta}{4m}\gamma_z = 0. \tag{6.2}$$

Conditions (3.17) for the leading-order stream function in the core $\Psi_1^{(0)}$ reduce to the linear coupling relations

$$\partial_z \Psi_1^{(0)} = 0, \quad \Psi_1^{(0)} + \partial_r \Psi_1^{(0)} = 2(1-m)m^{-1}\beta\eta \quad (r = 1). \tag{6.3}$$

The solution to the core problem (3.14), (6.3) in the form of Fourier representation

$$\Psi_1^{(0)} = \frac{1}{(2\pi)^{1/2}} \int_{-\infty}^{\infty} \psi_\alpha \, e^{i\alpha z} \, d\alpha, \tag{6.4}$$

can be written as

$$\left.\begin{aligned} \psi_\alpha &= \frac{2(1-m)m^{-1}\beta\eta_\alpha}{\Delta}[rI_0(\alpha r)I_1(\alpha) - I_1(\alpha r)I_0(\alpha)], \\ (\Delta(\alpha) &= \alpha\{[I_1(\alpha)]^2 - [I_0(\alpha)]^2\} + 2I_0(\alpha)I_1(\alpha)). \end{aligned}\right\} \tag{6.5}$$

The corresponding interfacial shear quantity was obtained by Papageorgiou *et al.* (1990)

$$\gamma_\alpha = 4(1-m)m^{-1}\beta\eta_\alpha \frac{\alpha[I_1(\alpha)]^2}{\Delta}. \tag{6.6}$$

Thus the small-amplitude evolution equation, which implies complete disregard for factors $(1+\eta)^n$ in (3.11), is that due to Papageorgiou *et al.* (1990), of the KS type with an additional dispersive term

$$\eta_t + \eta\eta_z + S(\eta_{zz} + \eta_{zzzz}) - \mathrm{i}\frac{\beta(m+2\beta)(1-m)}{2m^2\pi}\int_{-\infty}^{\infty}\frac{\alpha^2 I_1^2(\alpha)}{\Delta}\left\{\int_{-\infty}^{\infty}\eta(z',t)\,\mathrm{e}^{\mathrm{i}\alpha(z-z')}\,\mathrm{d}z'\right\}\mathrm{d}\alpha. \tag{6.7}$$

The shortest wavemodes with $\alpha \gg 1$ are overdamped by the dissipation and only behaviour of the coupling kernel for small and moderate wavenumbers $\alpha = O(1)$ is essential. A fraction which is responsible for dispersive properties of the last term in (6.7) has the following long-wave asymptotics (for $|\alpha| < 4$)

$$\frac{\alpha^2[I_1(\alpha)]^2}{\Delta} = 2\alpha + \tfrac{1}{6}\alpha^3 - \frac{\alpha^5}{576} + O(|\tfrac{1}{6}\alpha|^7), \tag{6.8}$$

and a proper approximation of the interfacial coupling (3.13) is

$$\gamma = \frac{2(1-m)}{3m}\beta(12\eta - \eta_{zz} - \tfrac{1}{96}\eta_{zzzz} + \ldots) \cong \frac{2(1-m)}{3m}\beta(12\eta - \eta_{zz}). \tag{6.9}$$

Therefore we expect behaviour of solutions of the modified (non-local) equation (6.7) to be close to that for the dissipative–dispersive equation considered by Kawahara and co-workers (Kawahara 1983; Kawahara & Toh 1988)

$$\eta_t + \eta\eta_\zeta + S(\eta_{\zeta\zeta} + \eta_{\zeta\zeta\zeta\zeta}) + c\eta_{\zeta\zeta\zeta} = 0, \tag{6.10}$$

where

$$c = \frac{\beta(1-m)(m+2\beta)}{6m^2}, \quad \zeta = z + 12ct. \tag{6.11}$$

Equations (6.7) and (6.10) can be rescaled by means of

$$\eta = SX, \quad t = \tau/S, \quad c = Sc_d, \tag{6.12}$$

which turns them into a form with single parameter c_d, coefficient of the dispersive term (DT)

$$X_\tau + XX_\zeta + X_{\zeta\zeta} + X_{\zeta\zeta\zeta\zeta} + c_d\,\mathrm{DT} = 0, \tag{6.13}$$

where the integral DT in the exact case (6.6) should be taken with the kernel $6\{\alpha^2 I_1^2(\alpha)/\Delta\} - 12\alpha$. Note that the weakly nonlinear interfacial equations (6.1), (6.7) and (6.10) admit symmetry $\{\eta \to -\eta, z \to -z\}$ while (3.19) and (3.11) do not: the factors $(1+\eta)^n$ (with $n = 1, 2, 3$) introduce influence of the wall.

In figures 17 and 18 we present results of simulations of (6.7) and (6.10) in the form (6.13) for the same 'random' initial conditions. At sufficiently high dispersion ($c_d \geqslant 0.3$) disturbances evolve into a pulse train which after a number of particle-like interactions tends to a steady propagation of identical (but not equidistant) travelling

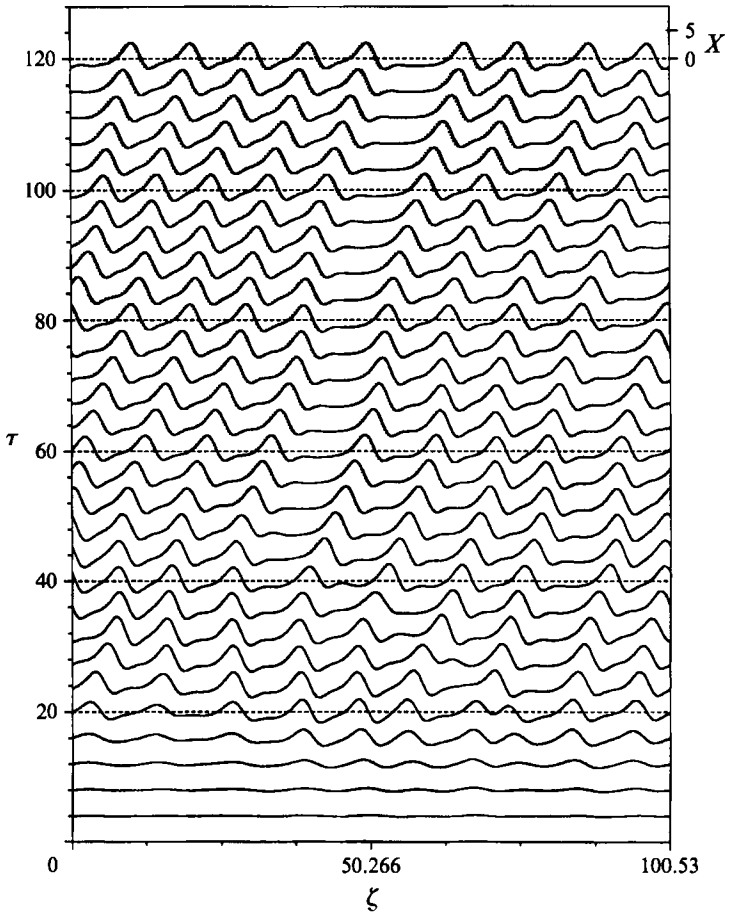

FIGURE 17. Development of an equilibrated pulse train in simulation of the modified KS equation with dispersion (6.13) for $c_d = 0.4$. Solid profiles correspond to the Kawahara equation, dotted profiles to the exact dispersive kernel (virtually coincide).

waves, see figure 17 for $c_d = 0.4$. This 'regularizing' effect of linear dispersion is the same as in the previous simulations and analysis of (6.13) by Kawahara (1983), Kawahara & Toh (1988) (see also Elphick *et al.* 1991; Chang *et al.* 1993). Solutions both for the exact and approximate kernels are extremely close. An example of semi-chaotic evolution of a cellular pattern for weaker dispersion ($c_d = 0.2$) is shown in figure 18. There are spatiotemporal discrepancies in the details of development (in particular, in phase shifts, similar to their appearance under small variations of other parameters, see Kawahara & Takaoka 1989), but evolution both for the exact and approximate dispersive kernel is attracted to very close low-dimensional inertial manifolds.

As previously mentioned, solutions of a highly nonlinear equation (3.19) are close to those of the KS equation (6.1) only for sufficiently small values of parameter $S < 0.04$. In the range of $S > 0.1$ behaviour of solutions differs both qualitatively and even by the order of amplitudes. It is necessary, therefore, for small values of $S \sim 0.1$ to solve equation (3.11) in its full form with the interfacial shear according to (6.6) and (6.9)

$$\eta_t + \{(1-48c)\,\eta - 36c\eta^2\}\,\eta_\zeta + S\{(1+\eta)^3(\eta_\zeta + \eta_{\zeta\zeta\zeta})\}_\zeta + c\{(1+\eta)^2\,\eta_{\zeta\zeta}\}_\zeta = 0, \quad (6.14)$$

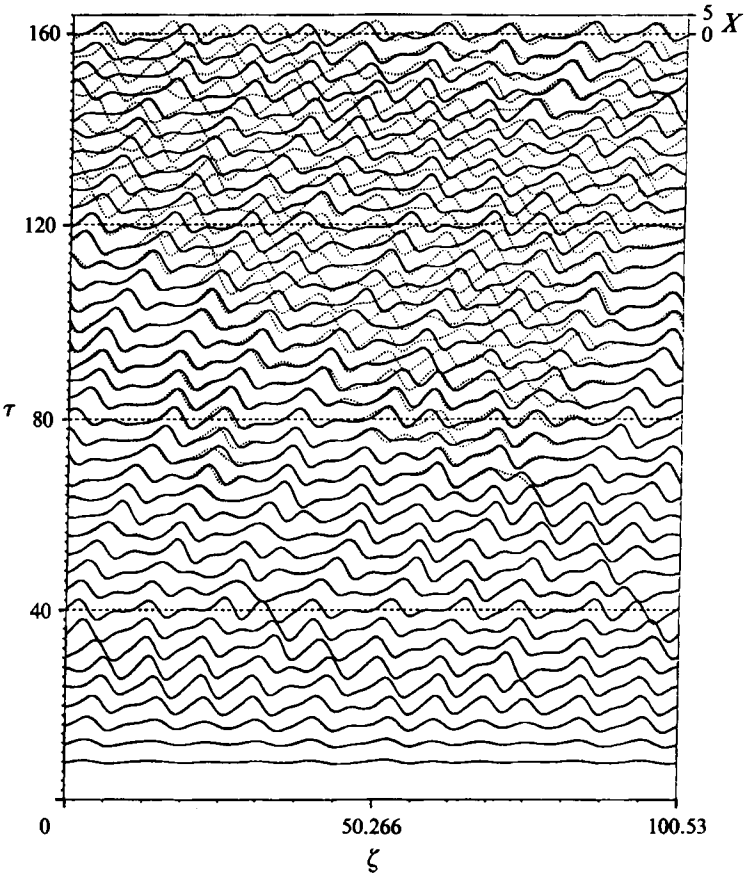

FIGURE 18. Chaotic evolution of a cellular pattern for $c_a = 0.2$ ($q = 16$). Notation as in figure 17. Behaviour is practically the same for the exact and approximate kernels except for specific details like phase shifts and defects disposition.

or at least a 'moderately' nonlinear $O(\eta^2)$ truncation of (3.11) and (6.14) (for $|\eta| < 0.3$)

$$\eta_t + (1-48c)\,\eta\eta_\zeta + S\{(1+3\eta)(\eta_{\zeta\zeta}+\eta_{\zeta\zeta\zeta\zeta}) + 3\eta_\zeta(\eta_\zeta+\eta_{\zeta\zeta\zeta})\} + c\{(1+2\eta)\,\eta_{\zeta\zeta\zeta} + 2\eta_\zeta\eta_{\zeta\zeta}\} = 0. \tag{6.15}$$

For the exact expression (6.6) one must replace $\eta_{\zeta\zeta}$ in the last term of (6.14) with the inverse Fourier transform of $6\{2-\alpha I_1^2(\alpha)/\Delta\}\,\eta_\alpha$. Solutions both for the exact and approximate kernel are still very close, and we further refer to a more compact form (6.14) (which also allows easier analysis and numerical solution).

Note that we can consider simplified forms (6.2), (6.7) and (6.15) of (3.11) and (6.14) in the *control parameters* range $S \ll 1, c \ll 1$ in a strictly asymptotic manner with proper rescaling (6.12) to the 'generic' equation (6.13) only for the case of very small S and c of the same order (and within the validity limitations expressed in terms of the *perturbation parameter* β). Otherwise, (6.14) and (6.15) should be regarded as *composite equations* (Van Dyke 1975) where it concerns sensitivity to reasonably small S and c. Comparison of (6.15) with (6.10) and (6.13) shows that even for fairly small values of the coupling parameter (6.11) $K = 12c \sim 0.1\,(c \sim 10^{-2})$, some substantial contribution to the convective term can be missed in a 'straightforward' derivation of

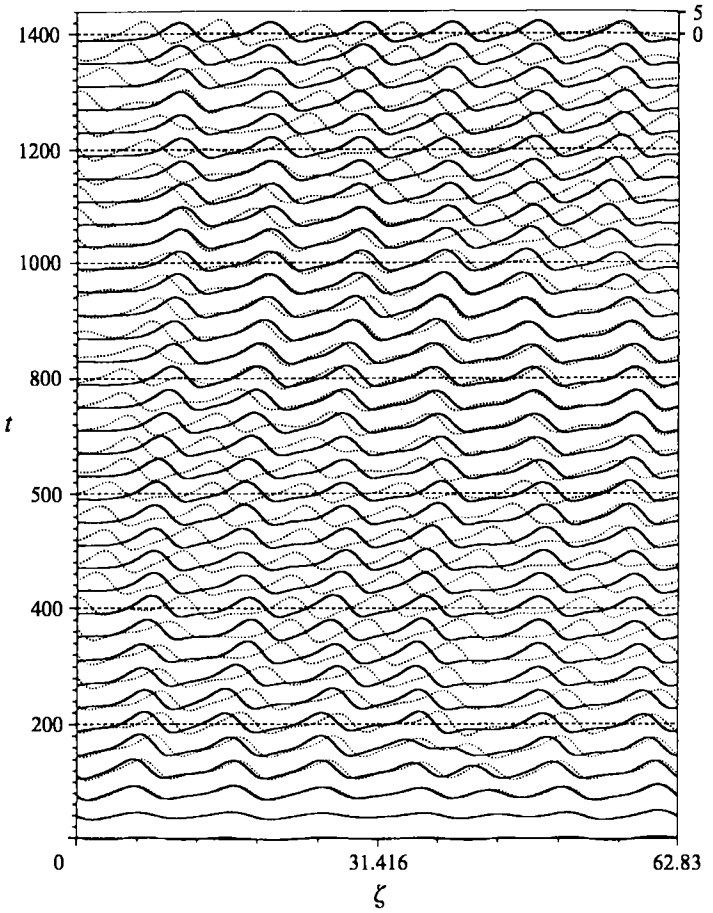

FIGURE 19. Evolution governed by (6.15) for $S = 0.05$, $c = 0.01$ (solid profiles). Dotted profiles show semi-chaotic solution to the weakly nonlinear equation (6.16) for the same S and c.

the small-amplitude equations (6.2) and (6.10), especially in the case of less viscous annulus ($m < 1$), when c is positive. The weakly nonlinear version of (6.14) should be written as

$$\eta_t + (1-48c)\,\eta\eta_\zeta + S(\eta_{\zeta\zeta} + \eta_{\zeta\zeta\zeta\zeta}) + c\,\mathrm{DT} = 0. \tag{6.16}$$

Thus, for physically reasonable magnitudes of the film thickness ratio $\beta = 0.005$–0.1, and $m < 1$ one must consider the canonic form (6.13) of the dissipative–dispersive equation under modified interfacial renormalization

$$X = (1-48c)\,\eta/S, \quad \tau = St, \quad c_d = c/S. \tag{6.17}$$

A rough judgement concerning the importance of (non-weakly) nonlinear effects in (6.14) may be based on the magnitude of a modified parameter (3.12): $S_c = S/|1-48c|$. Recall that there is a lower constraint on the validity of (3.11), (3.20) and (6.14)–(6.16) which can be stated here as $S_c/\beta^2 \gg 1$, in order to keep intact the capillarity-set scales. This narrows down the window where the weakly nonlinear approach seems justified. In figure 19 we present examples of the simulation (6.15), and (6.7) in the corrected form (6.16) – with the same initial conditions for $S = 0.05$ – in the case of low dispersion ($c = 0.01$; $S_c = 0.095$). It demonstrates that higher nonlinearity brings about

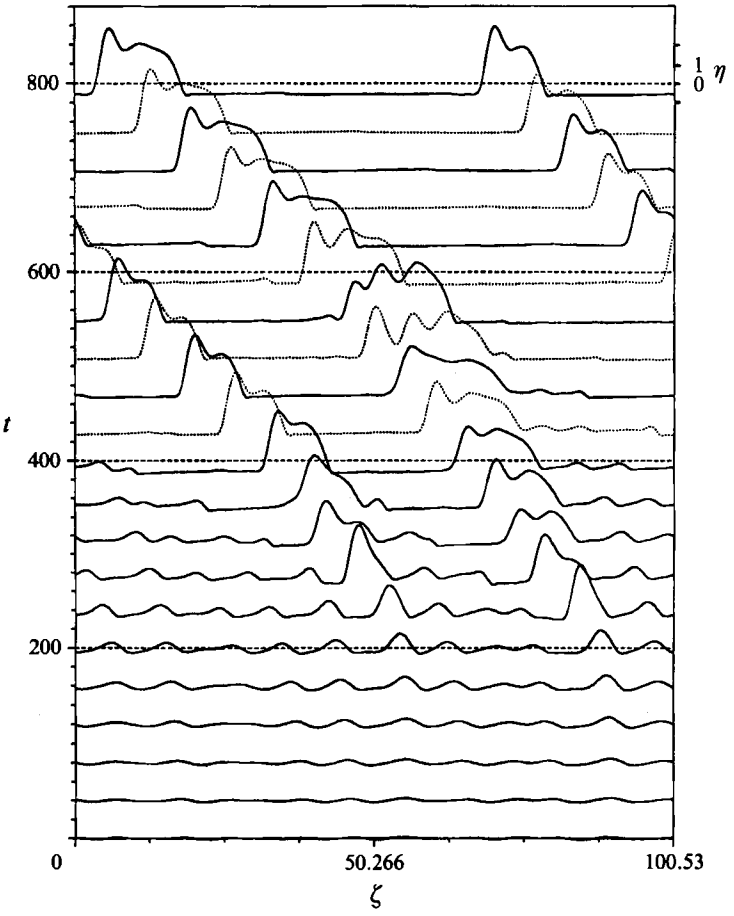

FIGURE 20. Development of the multi-peaked structures in simulation of (6.14) for $S = 0.05$ and $c = 0.015$ ($q = 16$). Dotted profiles are plotted at certain times for better distinguishability.

stabilization of the defect-mediated irregularities in (6.7) and development of a steady pulse train.

Figure 20 shows the simulation of (6.14) for a yet weaker stabilizing convective term and relatively high dispersion: $S = 0.05$, $c = 0.015$ ($S_c = 0.179$). Initially, developing waves stick together into pulseforms with two and three humps (of double and triple width, respectively), and eventually such inelastic interactions can result in the formation of broad bridges which separate elongated slugs of the core fluid.

Figure 21 shows evolution governed by (6.14) for stronger surface tension and weaker coupling: $S = 0.1$ and $c = 0.008$ ($S_c = 0.163$). Dispersion contributes to the formation of a large singular pattern that occurs after a number of particle-like interactions. This structure which develops at $t > 460$ grows like an approximate blow-up solution to (6.14) as intermediate asymptotics

$$h = 1+\eta = \frac{B(\xi)}{(t_*-t)^{\omega}}, \quad \xi = \zeta-\zeta_p, \tag{6.18}$$

where ζ_p denotes the tip location and $\omega \cong \frac{1}{3}$, see dependence for the peak's height $h_m = h(\zeta_p)$ in figure 21 (*b*). This behaviour, which leads the system beyond the premises of validity, is different from the cascade growth in evolution governed by (3.20) that we

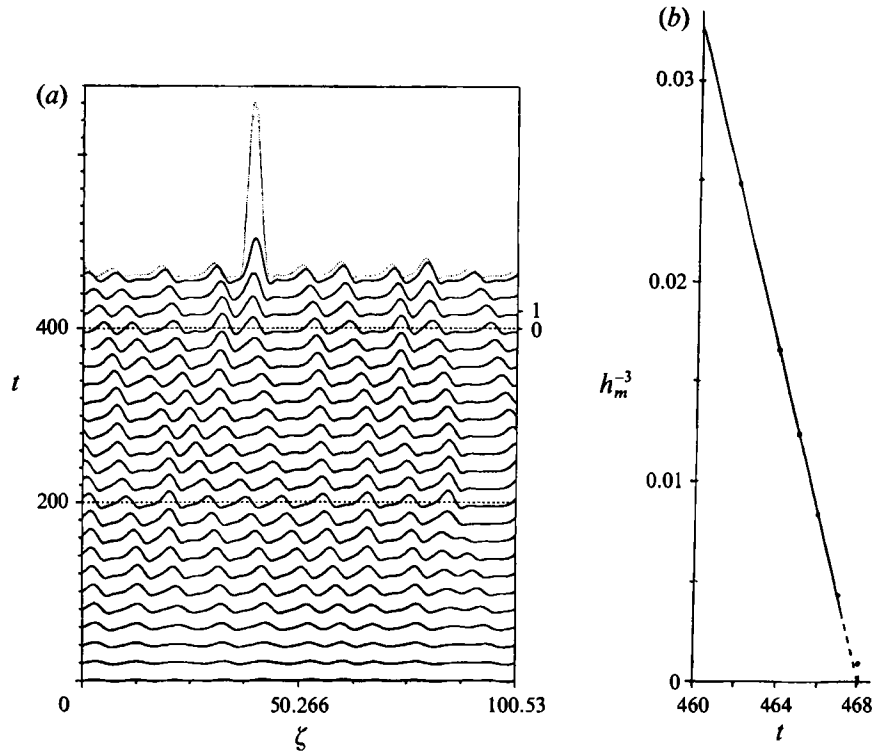

FIGURE 21. (*a*) Evolution for $S = 0.1$ and $c = 0.008$ that leads to blow-up. Solid profiles are shown at time intervals $\Delta t = 20$. Dotted profile is at $t = 468$. (*b*) Time dependence for identifying the peak's growth with finite-time singularity (6.18). The solid line represents an intermediate self-similar stage.

described in §4. Although (3.20) may have an approximate blow-up solution of the same form (6.18), we never observed the large-amplitude explosive growth (without any mergers in simulations for that decoupled equation. Kalliadasis & Chang (1994) attempted to describe the pulse growth in the evolution governed by the film-on-fibre equation (3.21) by approximate solutions in the form (6.18). However, their interpretation concerns a intermediate stage: $(h < 3, |t_* - t| \sim 1)$ of the primary instability development, when the convective term (neglected to achieve self-similarity) is in fact of the same order as those left. Our extensive simulations of the same equation (3.21) with various small-amplitude initial conditions (partly presented in Kerchman & Frenkel 1994) demonstrated that except for a comparatively short stage of primary development, the pulse growth for $S_g > 1$ is predominantly due to coalescences. Intermediate blow-up behaviour (6.18) for (6.14) may be of the same nature as for nonlinear dispersive equations of KdV type (see e.g. Bona & Saut 1993).

Stronger interfacial shear (when $c \geqslant 0.04$) brings nonlinear stabilization even for $S = 0.2$–0.3. Both components of the convective term enter in (6.14) with negative coefficients, and the appropriate reference frame (6.11) moves far slower than the unperturbed interface, with a factor $(1–12c)$. Evolution in figure 22 for $S = 0.15$ and $c = 0.06$ ($S_c = 0.08$ and high dispersion with $c_a = c/S = 0.4$) settles to a lattice of inverted saw-tooth pulses (note that in this range of c, transformation (6.17) to the normalized weakly nonlinear form (6.13) implies reflection with respect to the unperturbed interface $\eta = 0$). Stronger surface tension and low dispersive coefficients promote limited mergers of structures and the formation of larger core bulges

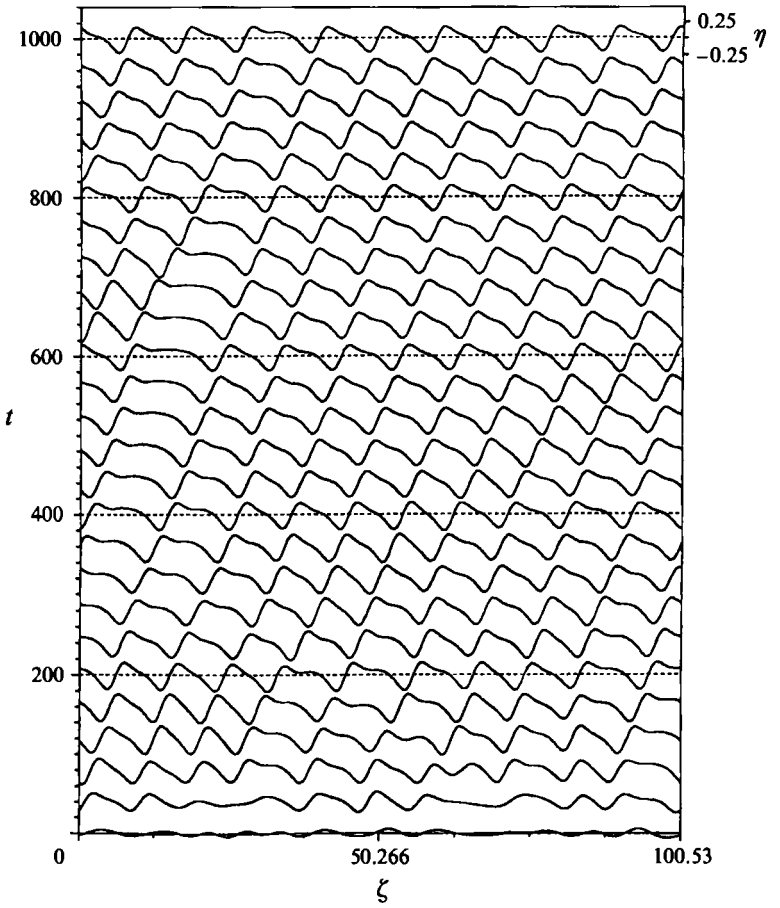

FIGURE 22. Regular train of inverted pulses for $S = 0.15$ and $c = 0.06$.

('negative pulses') which may approach the wall, as in figure 23. This pattern resembles 'bamboo waves' observed by Bai *et al.* (1992), but their experiments were performed with larger Reynolds numbers when inertial terms are significant (in particular, it results in shortening of unstable wavelengths.) It should be noted that strong viscosity stratification ($m < \beta$) reduces growth rates of the linearly unstable wavemodes $\alpha < 1$ (Hammond 1983; Hu & Joseph 1989; Joseph & Renardy 1993), and correspondingly the effective value of parameter S in (6.14) and (6.15), roughly speaking to $S' = fS$ where $f = f(\beta/m)$, $0.3 < f < 1$.

In the case of less viscous core fluid the coefficient (6.11) is negative: $c \cong -\frac{1}{6}\beta$ for $m \gg 1$, and according to (6.15) and (6.16) the interfacial shear has stabilizing effect for $S = O(\beta)$.

The general case $\mathbb{R}_1 \sim 1$ can be considered in a similar way by replacing the kernel in (6.6) with the complex-valued one which corresponds to the Orr–Sommerfeld equation (and is expressed by means of Kummer function in Frenkel 1988 and Georgiou *et al.* 1992). Inertia of the core flow contributes not only to the convective term and dispersion, but also to dissipative effects in the interfacial shear. Cross-influence of the parameters makes study of the relative importance of dispersion and dissipation more complicated.

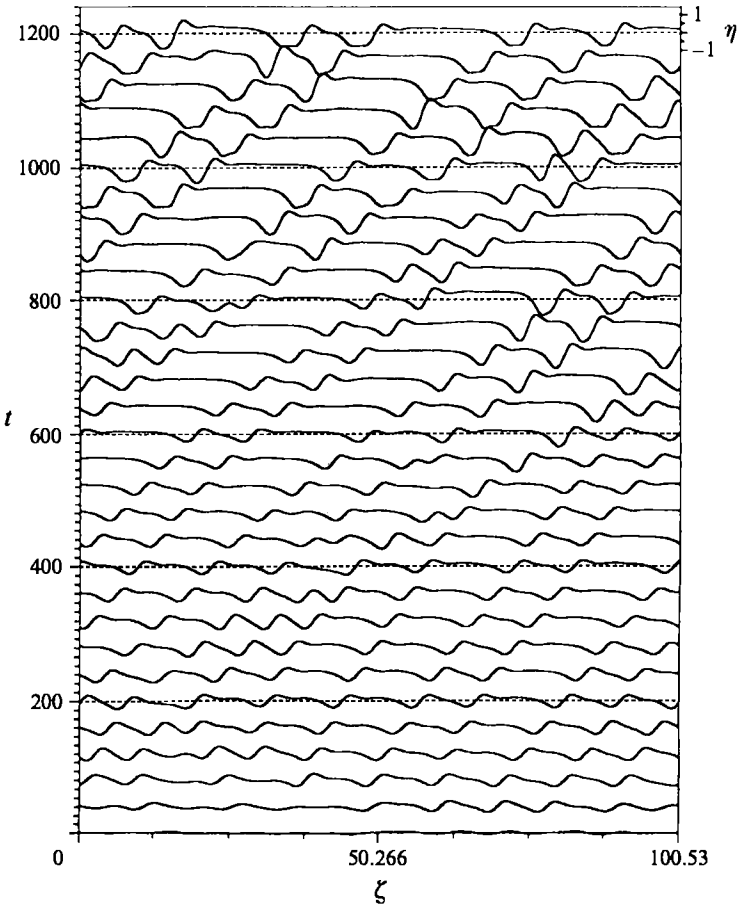

FIGURE 23. Formation of the 'negative solitary waves' (bulges of the core) in a strongly coupled CAFF for $S = 0.2$ and $c = 0.05$ ($q = 16$).

7. Summary and concluding remarks

We have developed a nonlinear theory of undulating interfaces in a core–annular flow in the limit of thin annulus: $\beta = (\bar{R}_2 - \bar{R}_1)/\bar{R}_1 \ll 1$. Capillary pressures at the interface are supposed to be high enough to set orders of magnitudes in the film flow with a major spatial scale of the order of linearly unstable wavelengths (about an undisturbed circumference). This allows us to analyse perturbed flow by a lubrication-type approximation for thin annular film. We derive a leading-order nonlinear equation (3.11) which describes development of interfacial disturbances up to the amplitudes of the order of unperturbed film thickness. Shear coupling with the core flow depends on the viscosity ratio $m = \bar{\mu}_2/\bar{\mu}_1$, and enters in the nonlinear terms of the equation as well. Long-time interfacial evolution governed by (3.11) and its particular case (3.20) demonstrate rich dynamics of coherent structures which sharply depend on the control parameter $S = \beta^3\bar{\sigma}/(3\bar{\mu}_2\bar{W}_{if}) \sim \beta^2/\mathbb{C}$, where $\bar{W}_{if}$ is the velocity of undisturbed interface, and $\mathbb{C}$ is the capillary number, $\mathbb{C} \ll \min\{1, m\}$. In narrow regions of the parameter space, where weakly nonlinear versions of (3.20) and (3.11) are valid, evolution is attracted to the KS-type chaos and the dispersion-regularized wavetrains respectively – thus keeping the interfacial disturbances at small amplitudes. Nonlinearities in the dissipative (and quasi-dispersive) terms change the character of

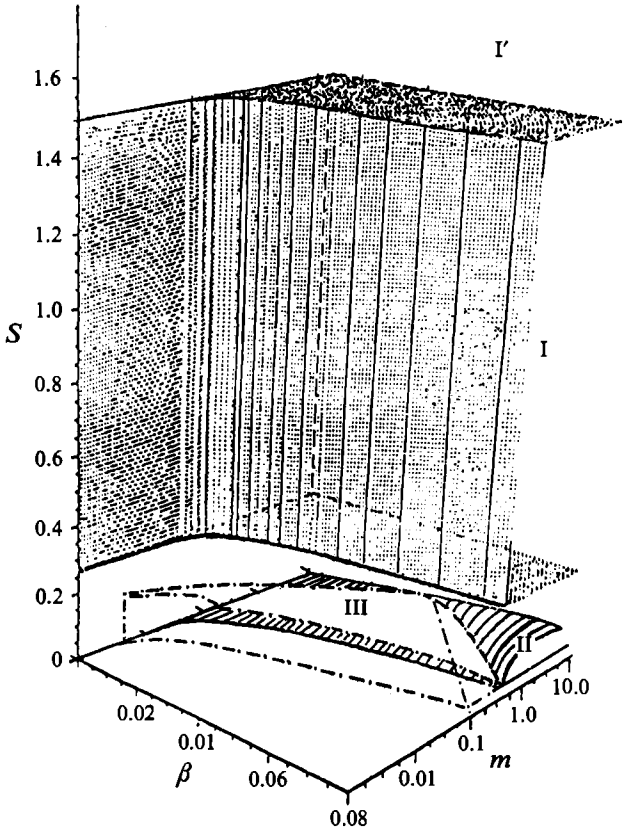

FIGURE 24. Sketch of the parameter space with regions corresponding to different flow conditions (m-axis is in a logarithmic scale). Inside the 'slab' (I) with a dotted boundary: $m \geqslant \beta^{1/2}$, $1.5 > S > 0.2$, evolution governed by (3.20) leads to the formation of thick-film non-uniformities via cascade absorption. In the domain (I′) above, extreme film thinning may occur too. Within the slender wedge (II): $0.04 > S_c \gg \beta^2$, $m \gg \beta$, a weakly nonlinear approach is valid. In the region (III) with dash–dotted edges the strongly nonlinear regimes with a significant interfacial shear are realized.

interactions of the pulse-like structures. In conjunction with the secondary instabilities it can result in the formation and growth of the large-scale inhomogeneities. These phenomena break the weakly nonlinear mechanisms of primary saturation proposed in Frenkel *et al.* (1987) and Papageorgiou *et al.* (1990). The spatial non-uniformities in an extended system for certain conditions are asymptotically bounded (quasi-)regular patterns, but more often they eventually lead the configuration out of geometric and physical limitations of the thin annular film model.

Figure 24 depicts schematics of regions in the space of basic parameters $\{\beta, m, S\}$ which correspond to various regimes of CAFF we were able to find. For $S > 0.2$ and the viscosity ratio m sufficiently larger than the thickness ratio ('slab' I with dotted boundary and the region I′ above it) one can neglect coupling with the core and consider evolution governed by (3.20) (the same is true in some subregions below around the plane $m = 1$ and for $m \gg 1$). Development of the interfacial disturbances in this range of parameters almost inevitably leads to a virtual breakup of the perfect CAF – mainly due to coalescences and the 'topological' instability of thick-film collars. This is in a good agreement with experimental data by Aul & Olbricht (1990).

Within a slender wedge II with a shaded top: $\beta > S \gg \beta^2, m \gg \beta$, the weakly nonlinear equation (6.13), (6.16) is valid.

In the case of less viscous annular film, the shear coupling with the core flow plays an important role even for fairly small values of the linking parameter $K = 2\beta(1-m)(m+2\beta)/m^2 \sim 0.1$. Involvement of the core changes the character of perturbation flow in the film by contributing both to the convective term of the equation and the (nonlinear) dispersion-like effects. The effects of surface tension and of interfacial shear are fundamentally combined but may be roughly evaluated in terms of modified parameters $S_c = S/|1-4K|$ and $c_d = c/S$. The modified weakly nonlinear equation (6.16) is valid only for $S_c < 0.04$. Moderate coupling when $K = 0.1$–0.3 affects in a disbalancing way even for $S \sim 0.05$ owing to effective reduction of the stabilizing convective term. A 'ceiling', above which large structures are formed and the CAF eventually collapses, is found to correspond $S_c = 0.1$–0.14. The region below is roughly shown in figure 24 as a 'scoop' III with the dot-dashed edges. Stronger interfacial shear ($K > 0.4$) brings stabilization to a train of inverted pulses (part of region III which is closer to its 'face' for $\beta = 0.03$–0.1). In the rest of the parameter space: $m \sim \beta$ for $S = O(1)$ or $m \ll \beta$ for any S – either nonlinear terms in the interfacial conditions for the core or inertial terms in the flow equations are essential.

CAF with a density stratification can be analysed by employing additional parameters (see Joseph & Renardy 1993)

$$l = \frac{\bar{\rho}_2}{\bar{\rho}_1}, \quad Bo = \frac{(l-1)\bar{\rho}_1}{\bar{\sigma}} \bar{g} \bar{R}_1^2, \quad F_g = F - 1 = \frac{\bar{F}}{\bar{\rho}_1 \bar{g}} - 1, \tag{7.1}$$

– the latter is important in the case of vertical CAF (z-axis is upwards).

For small Bond numbers $Bo \ll 1$ the difference of densities in a horizontal CAFF can be neglected. Density stratification in a vertical CAFF contributes to the second-order effects for the linear stability and weakly nonlinear interfacial waves (Georgiou *et al.* 1992; Smith 1989) as compared with the viscosity stratification ones. Strongly nonlinear interfacial waves in a general case of vertical CAFF can be described by the same leading-order equation (3.11) and its particular cases where parameters are based on the effective pressure gradient $\bar{F}_g = \bar{F} - \bar{\rho}_1 \bar{g}$. (This allows physical modelling of the perfect pressure-driven CAFF at low Reynolds numbers by a vertical cocurrent upward flow with the same value of parameter S in a tube of larger radius when $l \approx 1$ and F_g is relatively small.) The exception is for very small magnitudes of F_g when $\beta|l-1|/F_g$ is of order one. In this special case the convective term of a leading-order equation contains additional cubic nonlinearity due to the gravity contribution, and certain distinctive features of the large-amplitude interfacial evolution appear in the countercurrent flow for $S > 0.2$ (Frenkel & Kerchman 1994).

The work was initiated and partially done at the University of Alabama, Tuscaloosa, and supported in part by the US DOE under Grant DE-FG05-90ER14100. I wish to thank A. L. Frenkel for stimulating discussions at the onset of this work. The author has also benefitted from helpful comments by an anonymous reviewer.

REFERENCES

Amick, C. J. & Toland, J. F. 1992 Solitary waves with surface tension I: trajectories homoclinic to periodic orbits in four dimensions. *Arch. Rat. Mech. Anal.* **118**, 37–69.

Aul, R. W. 1989 The motion of drops and long bubbles through small capillaries: coalescence of drops and annular film stability. PhD thesis, Cornell University. Ithaca, NY.

Aul, R. W. & Olbricht, W. L. 1990 Stability of a thin annular film in a pressure-driven, low Reynolds number flow through a capillary. *J. Fluid Mech.* **215**, 585–599.

BAI, R., CHEN, K. & JOSEPH, D. D. 1992 Lubricated pipelining, stability of core–annular flow. Part 5. Experiments and comparison with theory. *J. Fluid Mech.* **240**, 97–132.

BENNEY, D. J. 1966 Long waves in liquid films. *J. Maths & Phys.* **45**, 150–155.

BONA, J. L. & SAUT, J.-C. 1993 Dispersive blowup of solutions of generalized Korteweg–de Vries equations. *J. Diffl Equat.* **103**, 3–57.

BRETHERTON, F. P. 1961 The motion of long bubbles in tubes. *J. Fluid Mech.* **10**, 166–188.

CHANG, H.-C., DEMEKHIN, E. A. & KOPELEVICH, D. I. 1993 Laminarizing effects of dispersion in an active–dissipative nonlinear medium. *Physica* D **63**, 299–320.

CHEN, K. & JOSEPH, D. D. 1991 Long wave and lubrication theories for core–annular flow. *Phys. Fluids* A **3**, 2672–2679.

COLLET, P., ECKMANN, J.-P., EPSTEIN, H. & STUBBE, J. 1993 Global attracting set for Kuramoto–Sivashinsky equation. *Commun. Math. Phys.* **152**, 203–214.

CONSTANTIN, P., FOIAS, C., NICOLAENKO, B. & TEMAM, R. 1989 *Integral Manifolds and Inertial Manifolds for Dissipative Partial Differential Equations.* Springer.

COULLET, P. & LEGA, J. 1988 Defect-mediated turbulence in wave pattern. *Europhys. Lett.* **7**, 511–516.

CROSS, M. C. & HOHENBERG, P. C. 1993 Pattern formation outside of equilibrium. *Rev. Mod. Phys.* **65**, 851–1112.

ELPHICK, C., IERLEY, G. R., REGEV, O. & SPIEGEL, E. A. 1991 Interacting localized structures with Galilean invariance. *Phys. Rev.* A **44**, 1110–1122.

EVERETT, D. H. & HAYNES, J. M. 1972 Model studies of capillary condensation. I. Cylindrical pore model with zero contact angle. *J. Colloid Interface. Sci.* **38**, 125–137.

FRENKEL, A. L. 1988 Nonlinear saturation of core-annular flow instabilities. *Proc. 6th Symp. on Energy Engineering Sciences.* Argonne, IL, US Dept of Energy, pp. 100–107.

FRENKEL, A. L. 1992 Nonlinear theory of strongly undulating thin films flowing down a vertical cylinder. *Europhys. Lett.* **18**, 583–588.

FRENKEL, A. L. & KERCHMAN, V. I. 1994 On large-amplitude waves in core–annular flows. *Proc. 14th IMACS Congress on Computations and Applied Mathematics.* Atlanta, 1994, vol. 2, pp. 397–400.

FRENKEL, A. L., BABCHIN, A. J., LEVICH, B. G., SHLANG, T. & SIVASHINSKY, G. I. 1987 Annular flow can keep unstable flow from breakup: nonlinear saturation of capillary instability. *J. Colloid Interface. Sci.* **115**, 225–233.

GAUGLITZ, P. A. & RADKE, C. J. 1988 An extended evolution equation for liquid film breakup in cylindrical capillaries. *Chem. Engng Sci.* **43**, 1457–1465.

GEORGIOU, E., MALDARELLI, C., PAPAGEORGIOU, D. T. & RUMSCHITZKI, D. S. 1992 An asymptotic theory for the linear stability of a core–annular flow in the thin annular limit. *J. Fluid Mech.* **243**, 653–677.

GJEVIK, B. 1970 Occurrence of finite-amplitude surface waves on falling liquid films. *Phys. Fluids* **13**, 1918–1925.

GOREN, S. L. 1962 The instability of an annular thread of fluid. *J. Fluid Mech.* **27**, 309–319.

HALPERN, D. & GROTBERG, J. B. 1992 Fluid-elastic instabilities of liquid-lined flexible tubes. *J. Fluid Mech.* **244**, 615–632.

HAMMOND, P. S. 1983 Nonlinear adjustment of a thin annular film of viscous fluid surrounding a thread of another within a circular cylindrical pipe. *J. Fluid Mech.* **137**, 363–384.

HICKOX, C. 1971 Instability due to a viscosity and density stratification in axisymmetric pipe flow. *Phys. Fluids* **14**, 251–262.

HOHENBERG, P. C. & SHRAIMAN, B. I. 1989 Chaotic behavior of an extended system. *Physica* D **37**, 109–115.

HU, H. H. & JOSEPH, D. D. 1989 Lubricated pipelines: stability of core–annular flow. Part 2. *J. Fluid Mech.* **205**, 359–396.

HYMAN, J. M., NICOLAENKO, B. & ZALESKI, S. 1986 Order and complexity in the Kuramoto–Sivashinsky model of weakly turbulent interfaces. *Physica* D **23**, 265–292.

IOOSS, G. & ROSSI, M. 1989 Nonlinear evolution of the two-dimensional Rayleigh–Taylor flow. *Euro. J. Mech.* B *Fluids* **8**, 1–22.

JOHNSON, M., KAMM, R. D., HO, L. W., SHAPIRO, A. & PEDLEY, T. J. 1991 The nonlinear growth of surface-tension-driven instabilities of a thin annular film. *J. Fluid Mech.* **233**, 141–156.

JOO, S. W. & DAVIS, S. H. 1992 Irregular waves on viscous falling films. *Chem. Engng Commun.* **38**, 111–123.

JOSEPH, D. D. & RENARDY, Y. 1993 *Fundamentals of Two-Fluid Dynamics, vol. II: Lubricated Transport, Drops, and Miscible Liquids*. Springer.

KALLIADASIS, S. & CHANG, H.-C. 1994 Drop formation during coating of vertical fibres. *J. Fluid Mech.* **261**, 135–168.

KAWAHARA, T. 1983 Formation of saturated solitons in a nonlinear dispersive system with instability and dissipation *Phys. Rev. Lett.* **51**, 381–383.

KAWAHARA, T. & TAKAOKA, M. 1989 Chaotic behaviour of soliton lattice in an unstable dissipative–dispersive nonlinear system. *Physica* D **39**, 43–58.

KAWAHARA, T. & TOH, S. 1988 Pulse interactions in an unstable dissipative–dispersive nonlinear system. *Phys. Fluids* **31**, 2103–2111.

KERCHMAN, V. I. & FRENKEL, A. L. 1994 Interactions of coherent structures in a film flow: simulations of a highly nonlinear evolution equation. *Theor. Comput. Fluid Dyn.* **6**, 235–254.

LIN, S.-P. 1969 Finite-amplitude stability of parallel flow with a free surface. *J. Fluid Mech.* **36**, 113–126.

LIN, S. P. & LIU, W. C. 1975 Instability of film coating of wires and tubes. *AIChE J.* **21**, 775–782.

LIU, J. & GOLLUB, J. P. 1994 Solitary wave dynamics of film flows. *Phys. Fluids* **6**, 1702–1712.

MIESEN, R. H. M., BEJNON, G., DUJVESTIN, P. E. M., OLIEMANS, R. V. A. & VERBEGGEN, T. M. M. 1992 Interfacial waves in core–annular flow. *J. Fluid Mech.* **238**, 97–117.

NEWHOUSE, L. A. & POZRIKIDIS, C. 1992 The capillary instability of annular layers and liquid threads. *J. Fluid Mech.* **242**, 193–209.

OOMS, G., SEGAL, A., VAN DER WEES, A. J., MEERHOFF, R. & OLIEMANS, R. V. A. 1984 A theoretical model for core–annular flow of a very viscous oil core and a water annulus through a horizontal pipe. *Intl J. Multiphase Flow* **1**, 41–60.

PAPAGEORGIOU, D. T., MALDARELLI, C. & RUMSCHITZKI, D. S. 1990 Nonlinear interfacial stability of core–annular film flows. *Phys. Fluids* A **2**, 340–352.

PARK, C. W. & HOMSY, G. M. 1984 Two-phase displacement in Hele-Shaw cells: theory. *J. Fluid Mech.* **139**, 291–308.

PREZIOSI, L., CHEN, K. & JOSEPH, D. D. 1989 Lubricated pipelining: stability of core–annular flow. *J. Fluid Mech.* **201**, 323–356.

PUMIR, A., MANNEVILLE, P. & POMEAU, Y. 1983 On solitary waves running down an inclined plane. *J. Fluid Mech.* **135**, 27–50.

QUÉRÉ, D. 1990 Thin films flowing on vertical fibers. *Europhys. Lett.* **13**, 721–725.

RAYLEIGH, LORD 1902 On the instability of cylindrical fluid surfaces. In *Scientific Papers*, vol. 3, pp. 594–596. Cambridge University Press.

SCHWARTZ, L. W., PRINCEN, H. M. & KISS, A. D. 1986 On the motion of bubbles in capillary tubes. *J. Fluid Mech.* **172**, 259–275.

SMITH, M. K. 1989 The axisymmetric long-wave instability of a concentric two-phase pipe flow. *Phys. Fluids* A **1**, 494–506.

VAN DYKE, M. 1975 *Perturbations Methods in Fluid Mechanics*. Parabolic Press. Stanford.